ELSEVIER

Biophysical Chemistry 117 (2005) 155 – 171

Biophysical Chemistry

http://www.elsevier.com/locate/biophyschem

Cholesterol reduces membrane electroporation and electric deformation of small bilayer vesicles

Sergej Kakorin, Ute Brinkmann, Eberhard Neumann*

Physical and Biophysical Chemistry, Faculty of Chemistry, University of Bielefeld, P.O. Box 100 131, D-33501 Bielefeld, Germany

Received 15 March 2005; received in revised form 4 May 2005; accepted 4 May 2005
Available online 31 May 2005

Abstract

Electric fields, similar in the order of magnitude of the natural membrane fields of cellular lipid/protein membranes, and chemical relaxation spectrometry can be used as tools to quantify the rigidifying effect of cholesterol in membranes. Small unilamellar vesicles of radius $a = 50 \pm 3$ nm, prepared form phosphatidylcholine, phosphatidylserine and phosphatidyl-glycerol in the molar ratio 1:1:1 and containing the optical lipid probe molecule 2-(3-diphenyl-hexatrienyl) propanoyl)-1-palmitoyl-*sn*-glycerol-3-phosphocholine (β-DPH pPC), serve as examples for curved lipid membranes. The data of electrooptical turbidity and absorbance relaxations at the wavelength $\lambda = 365$ nm are analysed in terms of membrane bending rigidity κ and membrane stretching modulus K. Both κ and K increase with increasing mole fraction x of cholesterol up to $x = 0.5$. The cholesterol induced denser packing of the lipids reduces the extent of both membrane electroporation (ME) and electroelongation of the vesicles. Further on, cholesterol in the lipid phase and sucrose in the aqueous suspension reduce the extent of membrane undulation and electro-stretching.

Keywords: Membrane electroporation; Bilayer elasticity; Turbidity dichroism; Absorption dichroism; Vesicle electroelongation; Lipid rearrangements; Membrane cholesterol

1. Introduction

Enzyme catalysis and signal transmission are key functions of cellular membranes which are critically dependent on the mechanic and electric properties of the lipid phases. Traditionally, lipid bilayer vesicles serve as models for the planar and curved bilayer parts of the protein–lipid membranes of cells and organelles. It is well known that the steroid cholesterol is a general controller of the membrane fluidity which, too, affects membrane catalytic and transport functions. Structurally, cholesterol causes a denser packing of the lipid phase, thereby modulating the elasticity of membranes. Cholesterol is a central constituent of the (glyco-) sphingolipid-rich inner membrane micro-domains or rafts containing clusters of special proteins. Some plasma membranes contain cholesterol up to the mole fraction of $x = 0.5$.

It is still difficult to quantify the effect of cholesterol on the packing order in molecular terms. The planar steroid ring system of cholesterol with a 3-β-hydroxyl group and an alkyl side chain at position C17 is rigid and oriented with the long axis parallel to the hydrocarbon chains of the phospholipids. The hydroxyl group of cholesterol is located in the vicinity of the phospholipid ester carbonyl group; see, e.g., [1–4]. The solubility of cholesterol in various lipid bilayers depends on the type of the lipid head group, the length of the acyl chain and the number of double bounds. Primarily, the presence of cholesterol affects the inner-elastical properties of membranes; it thereby modulates the function of membrane-bound proteins, such as the ion-channel activity of the nicotinic acetylcholine receptor by agonists [5] or the motion of the rafts [6–8].

With respect to membrane elasticity, cholesterol decreases the elastic area stretching modulus, K [9–12].

* Corresponding author. Tel.: +49 521 106 20 53; fax: +49 521 106 29 81.
E-mail address: eberhard.neumann@uni-bielefeld.de (E. Neumann).

0301-4622/$ - see front matter © 2005 Elsevier B.V. All rights reserved.
doi:10.1016/j.bpc.2005.05.001

For instance, for stearoyl-oleoyl-phosphatidylcholine (SOPC) membranes the area stretching modulus is $K=0.2$ N m^{-1} [10]. For cholesterol containing SOPC membranes, the modulus K increases up to 0.6 N m^{-1}, similar to cholesterol in dimyristoyl-phosphatidylcholine (DMPC) membranes [9,13]. Cholesterol in SOPC membranes causes also an increase in the membrane bending rigidity from $\kappa(x=0)=0.9\cdot10^{-19}$ J up to $\kappa(x=0.5)=3.3\cdot10^{-19}$ J at the saturating mole fraction $x=0.5$ [11].

Molecular dynamics simulation shows that cholesterol condenses the lipid bilayer membrane. The average membrane area decreases with increasing cholesterol content, concomitant with an increase in the order of the hydrocarbon chains of the lipid molecules. Parallel to this ordering, the probability of gauche defects in hydrocarbon tails decreases [14]; apparently cholesterol restricts the conformational freedom of the acyl chains of the phospholipids in the liquid crystalline phase, thus decreasing the *trans*-gauche isomerizations [2]. Deuterium (2H) NMR data have shown that 30 mol% cholesterol in 1-palmitoyl-2-oleoyl-*sn*-glycero-3-phosphocholine (POPC) membranes at 25 °C increases the bilayer thickness from 2.58 nm to 2.99 nm [15]. At $x\geq0.1$ a progressive broadening of the thermal gel-to-fluid phase transition in 1-palmitoyl-2-oleoyl-phosphatidylethanolamine (POPE) [16]. The tighter molecular packing of the lipids in the presence of cholesterol leads to a reduction of the water content of the bilayer [17,18]. This dehydration decreases with increasing double bounds in the lipid acyl chains. The decay time constant of the fluorescence anisotropy of 1,6-diphenyl-1,3,5-hexatriene (DPH) and of 1-[4-(trimethylammonio) phenyl]-6-phenyl-1,3,5-hexatriene (TMA-DPH) decreases with increasing cholesterol concentration [19,20], suggesting an increased alignment of the membrane probes along the acyl chains (Fig. 1). However, the detailed molecular organization of cholesterol in different phospholipid bilayers is still a matter of debate [21,22].

Cholesterol is known to impede the electromechanical membrane permeabilization [9]. Here, we use the method of membrane electroporation (ME) to explore the rigidifying effect of cholesterol in curved lipid bilayer membranes. ME is an electric technique to render lipid and lipid–protein membranes porous and permeable, transiently and reversibly, by electric voltage pulses [23–25]. Specifically, we use relaxation spectrometric data in high electric fields in order to quantify the effect of cholesterol on electric pore formation in terms of positional changes of the optical lipid reporters β-DPH pPC in vesicle membranes. The DPH part of β-DPH pPC replaces one of the two hydrocarbon chains of the lipid molecule, representing thus an optically anisotropic indicator for positional changes in the lipid phase. It is recalled that both, electric absorbance dichroism and turbidity dichroisms, primarily reflect electro-elastic and electroporative vesicle elongation due to Maxwell stress [26,27]. As novelty, we here use absorbance and turbidity to monitor orientational changes of the optical reporter molecule β-DPH pPC in lipid bilayers of different contents of cholesterol. It is shown that the rigidifying effect of cholesterol can be also quantified in terms of positional changes of the optical lipid probe β-DPH pPC.

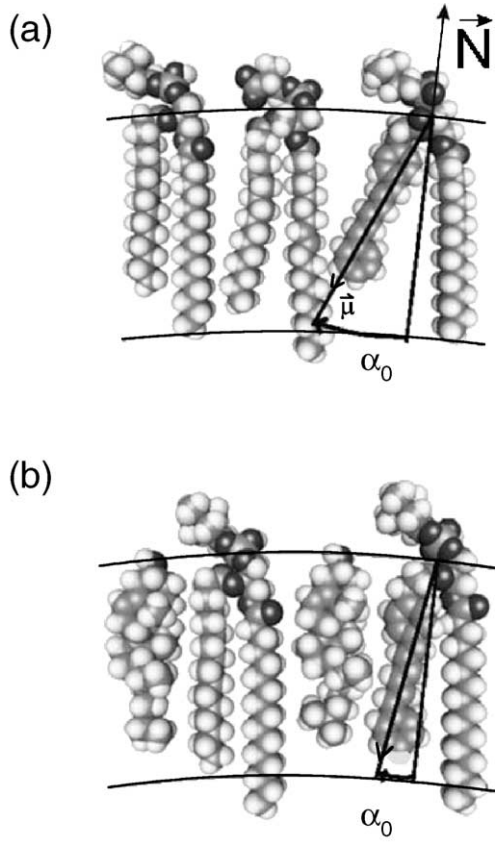

Fig. 1. Scheme for the rotational displacement of the lipid molecule β-DPH pPC in one monolayer of the bilayer: (a) in the absence and (b) in the presence of cholesterol. The angle α of the optical transition moment $\vec{\mu}$, parallel to the long axis of the chromophore β-DPH pPC and the membrane normal $\vec{N}$ (perpendicular to the membrane surface) decreases as a function of the mole fraction x of cholesterol; for instance, from $\alpha_0(x=0)=38°$ to $\alpha_0(x=0.15)=20°$ for salt-filled vesicles. The scheme refers to the electro-optical data of β-DPH pPC.

2. Materials and methods

2.1. Materials

Soybean phosphatidylcholine (PC, > 99% by weight), soybean phosphatidylglycerol (PG, > 98%) from Lipoid KG, phosphatidylserine (PS) from bovine brain extract type III; containing 80–85% PS and cholesterol (Chol, 99% by weight) from Sigma Chemie GmbH are used without further purification. PC and PG consist mainly of linolate (60%) and of oleate and palmitate (both total 13%). The lipid serving as optical probe is 2-(3-diphenylhexatrienyl)propanoyl)-1-palmitoyl-*sn*-glycerol-3-phosphocholine (β-DPH pPC) from Molecular Probes.

2.2. Unilamellar vesicle preparation

Small lipid vesicles ($30 \leq$ radius/nm ≤ 150) are readily prepared as unilamellar curved membranes [28] with geometrical curvatures that are similar to those encountered in invaginated biological plasma membranes and organelle vesicles. Pure unilamellar vesicles and vesicles doped with the lipid β-DPH pPC are prepared by the vesicle extrusion technique (VET, Ø=100 nm). Cholesterol is added to the mixture of PC, PG and PS in the molar ratio 1:1:1 in chloroform. The mixtures are dried using vacuum rotary evaporation. For the β-DPH pPC doped vesicles an adequate amount of PC has been replaced by β-DPH pPC dissolved in ethanol to obtain the molar ratio β-DPH pPC/lipid=1:200. During the vesicle preparation and the following electrooptic measurements the DPH-samples have been protected from light (photolysis) [28].

The dry lipid film (after evaporation) is resuspended in 0.2 mM NaCl and freeze-thawed five times in liquid nitrogen and in a water bath (30 °C) to obtain equilibration between trapped and bulk solution. The suspension is then extruded 21 times through polycarbonate membrane filters with a pore diameter of 100 nm (Avestin/Milsch, Germany) using a LiposoFast mini-extruder (Avestin/Milsch, Germany) to produce the low-salt vesicles of mean radius $a=50\pm3$ nm [28].

2.3. Salt-filled vesicles

For the preparation of salt-filled vesicles, the dry lipid film is resuspended in 0.5 M NaCl. After extrusion, the vesicle suspension is dialysed against 0.72 M sucrose solution of the same osmolarity to remove the external NaCl. Finally, the vesicle suspensions are diluted with degassed sucrose solution or with degassed 0.2 mM NaCl solution. The total lipid concentrations are $[L_T]=1$ mM and [β-DPH pPC]=5 μM, corresponding to a mole fraction x(β-DPH pPC)=0.005. Within 4–5 h after the preparation of vesicles, the electrooptical relaxations are unchanged [28]. We therefore can safely assume that the number of lipid molecules in the two membrane leaflets is constant as prepared, hence the spontaneous curvature of the membrane remains unchanged during the measurements.

2.4. Electrooptical relaxation spectrometry

2.4.1. The field-jump technique

Rectangular electric pulses of the duration $t_E=10$ μs and field strengths up to 8.5 MV m^{-1} are applied by cable discharge to a sample cell equipped with quartz windows and two parallel planar graphite electrodes [27], thermostated at $T=293$ K (20 °C). The distance between the electrodes can be accurately adjusted within $0.3 \leq h/mm \leq 0.5$, dependent on the conductivity of the vesicle suspension and the field strength [28]. Note, that at a pulse duration of $t_E=10$ μs and at field strengths $E \leq 8$ MV/m and for vesicle radii $a \leq 150$ nm, we may safely neglect vesicle–vesicle interactions, therefore there are no pearl-chain alignments [29].

The field-induced changes ΔOD in the optical density OD (or extinction) for plane-polarized light are measured at the wavelength $\lambda=365$ nm (Hg-line in vacuum; highest accuracy). The light intensity change ΔI^σ, caused by the electric pulse and measured at the polarization angle σ relative to the direction of the applied external field vector E, is related to the optical density change by:

$$\Delta OD^\sigma = OD^\sigma(E) - OD_0^\sigma = -\log(1 + \Delta I^\sigma / I^\sigma), \quad (1)$$

where $\Delta I^\sigma = I^\sigma(E) - I^\sigma$ is the light intensity change from I^σ (at $E=0$) to $I^\sigma(E)$ in the presence of E; OD^σ(E) and OD_0^σ are the optical densities at E and at $E=0$, respectively. Generally, $OD=A+T$, comprising both absorbance (A) and turbidity (T) along the light path length $A=1$ cm. At small concentrations of β-DPH pPC in the membrane (1 μM), the absorbance of the bilayer lipids does not affect the scattering of light by the vesicles. Therefore, the absorbance $A^\sigma = OD^\sigma(V,D) - OD^\sigma(V)$ of the reporter lipids in the bilayer of the vesicles is given by the difference between $OD^\sigma(V,D)$ of the doped vesicles and $OD^\sigma(V)$ of the vesicles without the reporter lipids, but at the same total lipid concentration and vesicle size. Since the initial value of the turbidity T_0 depends linearly on the lipid concentration up to $[L_T] \leq 5$ mM [28], there is no indications of multiple light scattering in the vesicle suspension at the smaller concentration $[L_T]=1$ mM.

2.4.2. Dichroitic and chemical contributions

The field-induced optical change ΔOD^σ is usually decomposed into a deformational/orientational part, ΔOD_{OR}^σ, and a structural/chemical part, ΔOD_{CH}^σ. In Appendix A it is recalled that, in line with Lambert–Beer's law for the absorbance, the orientational term refers to the respective positional change of the optical probes and the chemical term refers to the change in the environment of the optical transition moment of the chromophore [30]. Here we use the dilute solution approximation:

$$\Delta OD^\sigma = \Delta OD_{OR}^\sigma + \Delta OD_{CH}^\sigma. \quad (2)$$

The field-induced changes $\Delta OD^{\parallel}$ and $\Delta OD^{\perp}$ at the two light polarization modes $\sigma=0°$ ($\parallel$, parallel to the external field vector $\vec{E}$) and $\sigma=90°$ ($\perp$, perpendicular to $\vec{E}$) are given by $\Delta OD^{\parallel} = OD^{\parallel} - OD_0$ and $\Delta OD^{\perp} = OD^{\perp} - OD_0$, respectively. As outlined for the absorbance dichroism [30] both the consumptive dichroism ($\Delta A = \Delta A_{OR}^{\parallel} - \Delta A_{OR}^{\perp}$) and the conservative turbidity dichroism ($\Delta T = \Delta T_{OR}^{\parallel} - \Delta T_{OR}^{\perp}$) are originally defined for OD—changes of purely deformational/orientational origin [30]. The respective field-induced changes of the absorbance are calculated according to: $\Delta A_{OR}^{\parallel,\perp} = OD_{OR}^{\parallel,\perp}(V,D) - OD_{OR}^{\parallel,\perp}(V)$ and $\Delta A_{CH}^{\parallel,\perp} =$

$OD_{CH}^{\parallel,\perp}(V,D) - OD_{CH}^{\parallel,\perp}(V)$. It is recalled [30], that the (experimental) difference modes

$$\Delta OD^{-} = \Delta OD^{\parallel} - \Delta OD^{\perp}, \tag{3}$$

either for the case $\Delta OD^{-}=\Delta A^{-}$ or $\Delta OD^{-}=\Delta T^{-}$, are *not* the classical dichroisms ΔA and ΔT, respectively. The respective difference modes are explicitly given by:

$$\Delta T^{-} = \Delta T^{\parallel} - \Delta T^{\perp} = \Delta T + \left(\Delta T_{CH}^{\parallel} - \Delta T_{CH}^{\perp}\right)$$

$$\Delta A^{-} = \Delta A^{\parallel} - \Delta A^{\perp} = \Delta A + \left(\Delta A_{CH}^{\parallel} - \Delta A_{CH}^{\perp}\right). \tag{4}$$

Only in the case of small chemical contributions or if $\Delta T_{CH}^{\parallel} \approx \Delta T_{CH}^{\perp}$ and $\Delta A_{CH}^{\parallel} \approx \Delta A_{CH}^{\perp}$, we may approximate the difference modes by the classical dichroisms: $\Delta T^{-}=\Delta T$ and $\Delta A^{-}=\Delta A$ [31].

Analogous to the expression for ΔA_{CH} [32] we obtain:

$$\Delta OD^{+} \equiv \Delta OD_{CH} = \left(\Delta OD^{\parallel} + 2\cdot\Delta OD^{\perp}\right)/3, \tag{5}$$

or explicitly: $\Delta T^{+} \equiv \Delta T_{CH} = (\Delta T^{\parallel} + 2\cdot\Delta T^{\perp})/3$ and $\Delta A^{+} = \Delta A_{CH} = (\Delta A^{\parallel} + 2\cdot\Delta A^{\perp})/3$. The turbidity term ΔT^{+} generally refers to changes in the scattering cross section due to entrance of water and ions in the membrane, as well as to changes of vesicle volume. The absorbance term ΔA^{+} reflects modification of the immediate environment of the absorbing chromophore due to entrance of water and small ions in the bilayer surface. The conservative scattering dichroism ΔT as well as the consumptive absorbance dichroism ΔA, both are a quantitative measure of global shape deformations of the vesicles in the electric field pulse. Additionally, ΔA reflects the average position of the transition moments of optical membrane probes [27].

It is noted that the conventional birefringence refers per se to the difference in the two refractive indices (for the two polarization modes of the light) and is thus directly related to the difference modes ΔA^{-} and ΔT^{-}, respectively. In birefringence there is no independent chemical mode (ΔA^{+}, ΔT^{+}).

2.4.3. Solution conductivity

The conductometric measurements before and 5 min after application of the electric pulses are performed with a Knick digital conductometer. For the short pulse time (t_E=10 μs), electrode polarization effects and Joule heating are negligibly small. The initial conductivity is λ_0=4.1±0.2 mS m^{-1}.

3. Theory

3.1. Vesicle electrodeformation

3.1.1. Light scattering of vesicle suspensions

In most practical cases, the shape of an elongated vesicles may be approximated by a spheroid [33]. The field-induced vesicle elongation is described by an ellipsoid of revolution with the two principal semi-axes c and b, where $c>b$. Within the pulse time the long axis of the ellipsoids remains oriented parallel to the external field direction, because Maxwell stress elongates the vesicles in the direction of the external field [27].

In those cases, where the difference turbidity mode ΔT^{-} is not the conservative turbidity dichroism ΔT, the absolute value of the chemical mode $|\Delta T^{+}|$ is comparable with that of ΔT (> 0) and the difference $(\Delta T_{CH}^{\parallel} - \Delta T_{CH}^{\perp})$ in Eq. (4) contributes to ΔT. Therefore both ΔT^{-} and ΔT^{+} are used for the analysis in terms of a numerical code, solving the electromagnetic scattering problem for confocal coated spheroids by the separation of variables in a spheroidal coordinate system [34]. The numerical processing of the turbidity modes ΔT^{-} and ΔT^{+} yields the degree of electromechanical vesicle elongation expressed as the axis ratio $p=c/b$. Theoretically, the elongation of a spherical vesicle is either concomitant with an increase in the membrane surface area by, e.g., membrane stretching and electropores, or with a decrease of the intravesicular volume by efflux of internal medium through the membrane pores, or with both.

3.1.2. Elongation at constant vesicle volume

If the relative increase $\Delta S/S_0=(S-S_0)/S_0$ in the membrane surface area S occurs at constant internal volume $V_0=(4\pi/3)\cdot a^3=(4\pi/3)\cdot c^3/p_v^2$, the general expression for $\Delta S/S_0(p_v)$ can be approximated for the range $1 \le p_v \le 1.13$ 1.13 as [35]:

$$\frac{\Delta S}{S_0} \approx \frac{8}{45}(p_v - 1)^2, \tag{6}$$

where the parameter p_v is the axis ratio of the ellipsoid at constant volume and $S_0=4\pi\cdot a^2$ is the initial (projected) surface area of the spherical vesicle. See Fig. 2.

3.1.3. Elongation at constant membrane surface area

For the case of constant membrane surface area, including the area of membrane pores, the general expression for the volume change $\Delta V/V_0$ for small vesicle

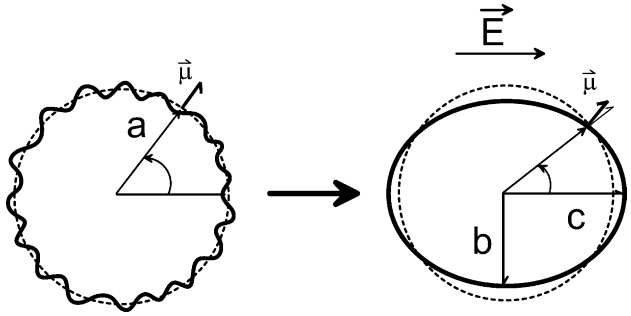

Fig. 2. Elongation of a vesicle at constant volume by field-induced smoothing of membrane undulations. The projected area $S_0=4\pi\cdot a^2$ refers to the dashed line. The elongation leads to the rotational displacement of the optical transition moment $\vec{\mu}$ of the chromophore β-DPH pPC in the membrane away from the direction of the external electric field.

elongations up to $1 \le p_s \le 1.10$, is approximated by [35,36]:

$$\frac{\Delta V}{V_0} \approx -\frac{4}{15}\cdot(p_s-1)^2, \tag{7}$$

where p_s is the axis ratio at constant surface. Since $p_s \ge 1$, elongation leads to a volume reduction. Generally, the vesicle deformation parameter $p=b/c$, Fig. 2, is represented by the sum [35]:

$$p = 1 + \Delta p_v + \Delta p_s, \tag{8}$$

where $\Delta p_v = p_v - 1$ and $\Delta p_s = p_s - 1$ are the increases in p at constant vesicle volume and at constant membrane surface area, respectively. For the case that $\Delta p_s \approx 0$, $p \approx 1 + \Delta p_v$ and p is solely a function of the increase ΔS in the membrane area.

3.1.4. Membrane stretching

In a rectangular electric field pulse, the time course of the surface change $\Delta S(t)$ reflects several processes: membrane stretching (MS), smoothing of thermal undulations (SU) and membrane electroporation (ME) [35]. The characteristic decay time τ_{MS} of membrane stretching (after removing of the stretching force) is given by [37]:

$$\tau_{MS} \approx \frac{\eta \cdot a}{K}, \tag{9}$$

where η is the solution viscosity and K the elastic area stretching modulus. For typical values of $\eta = 10^{-3}$ kg m^{-1} s^{-1} at $T=293$ K and $K=0.2$ N m^{-1}, Eq. (9) yields $\tau_{MS} \approx 0.25$ ns. This time constant is very small. Therefore membrane stretching can, for instance, not be kinetically resolved by the field-jump relaxation technique used here, where already the machine time is as large as $\tau_m = 70$ ns [35].

The increase in the vesicle surface area due to the membrane stretching is given by [35]:

$$\frac{\Delta S_{MS}}{S_0} = \frac{T_g + T_\ell}{K}, \tag{10}$$

where T_g and T_ℓ are components of the global and local Maxwell membrane tensions, respectively. As outlined in the appendix, the global tension T_g is caused by the global Maxwell stress on the vesicle exposed to an electric field (Eq. (A8)), leading to vesicle elongation, membrane stretching and smoothing of membrane undulations [31]. In contrast to T_g, the local Maxwell tension T_ℓ acts across the membrane, perpendicular to the membrane surface [9]. Since the lipid membrane behaves as a capacitor, T_ℓ can be expressed through the specific membrane capacity C_m; see Eq. (A9). Because the membrane is incompressible, T_ℓ, like T_g, tends to increase the membrane surface area by decreasing the membrane thickness. Differently to T_g, the local tension T_ℓ can not cause vesicle elongation or smoothing of membrane thermal undulations.

3.1.5. Smoothing of thermal undulations (SU)

In an electric field E, the characteristic time τ_{SU} of membrane smoothing (permitting the vesicle elongation) is given by [38]

$$\tau_{SU} \approx \frac{3\eta \cdot a^3}{\frac{48\cdot\kappa}{5} + \frac{3}{2}\sigma_o \cdot a^2 \cdot \left(1 + \frac{K}{\sigma_o + K/L}\right)} \tag{11}$$

where σ_0 is the membrane initial lateral tension, κ the bending rigidity of the membrane and $L = 8\pi\cdot\kappa/(k_B T)$ is a dimensionless smoothing constant. The area increase ΔS_{SU} is approximated by [38]:

$$\frac{\Delta S_{SU}}{S_0} = \frac{k_B T}{8\pi\cdot\kappa} \ln\left(1 + \frac{T_g}{(\pi\cdot\kappa/4\cdot a^2) + \sigma_0}\right) \tag{12}$$

where k_B is the Boltzmann constant and T the absolute temperature.

3.2. Membrane electroporation (ME)

As outlined previously [23,39], ME is structurally described as a state transition from (several) closed membrane states (C) to (several) porous states (P) according to the global reaction scheme $(C) \rightleftharpoons (P)$. The minimum reaction scheme for a consistent physical–chemical description, however, is the two-step cascade [40]:

$$C \rightleftharpoons C_1 \rightleftharpoons (P) \tag{13}$$

The first step $C \rightleftharpoons C_1$ is associated with the intrinsic equilibrium constant $K'_1 = [C_1]/[C] = k'_1/k'_{-1}$ and the intrinsic relaxation rate $1/\tau'_1 = k'_1 + k'_{-1}$, where the intrinsic rate constant k'_1 refers to the step $C \rightarrow C_1$ and k'_{-1} to the backward step $C \rightarrow C_1$. The data basis [35,40] suggests that the first step is rate-limiting in the coupling to the more rapid step $C_1 \rightleftharpoons (P)$ of the actual pore formation, associated with the intrinsic thermodynamic and kinetic parameters $K'_2 = [(P)]/[C_1]k'_2/k'_{-2}$ and $1/\tau'_2 = k'_2 + k'_{-2}$, respectively. Due to this particular coupling, there is only one kinetic normal mode with the (measured) relaxation time τ_2. The relaxation rate of this mode is given by [40]:

$$\frac{1}{\tau_2} = k_2 + k_{-2} = k'_1 + k'_{-1}\frac{1}{1 + K'_{-2}}. \tag{14}$$

Since ME is concomitant with an increase ΔS_{ME} in the membrane surface area S, the overall degree $f_2 = [(P)]/[C_0]$ of ME is expressed as

$$f_2 = f_2^0 = \frac{\Delta S_{ME}}{S_0} \tag{15}$$

where $f_2^0 = f_2(t=0)$ and the "concentration" sum is given by $[C_0] = [(P)] + [C_1] + [C]$.

The previous expression $K_p=[(P)]/[(C)]=k_p/k_{-p}$ [40] is now specified in terms of scheme Eq. (13), such that the *overall* poration–resealing equilibrium constant is given by [41]:

$$K_2=\frac{[(P)]}{[C_1]+[C]}=\frac{f_2}{1-f_2} \tag{16}$$

where $f_2=K_2/(1+K_2)$ replaces the previous $f_p=K_p/(1+K_p)$. Note that the measured overall constant $K_2=k_2/k_{-2}=K_2'\cdot K_2'\cdot K_1'/(1+K_1')$ is a combination of the intrinsic constants K_1' and K_2'.

From Eq. (14) it is seen that $k_2=k_1'$ and $k_{-2}=k_{-1}/(1+K_2')$, reflecting the experimental experience that always $K_p=K_2\ll 1$; here $K_2\approx 10^{-3}$ to 10^{-2} [25]. Obviously, $K_1'=k_1'/k_{-1}'\gg 1$ or $k_1'\gg k_{-1}'$ and $K_2'\ll 1$ or $k_2'\ll k_{-2}'$. Therefore, we use the appropriate approximation $K_2=f_2$, connecting the (experimental) overall apparent equilibrium constant with the measurable quantity f_2; e.g., by ΔS_{ME}, see Eq. (15). On the same line, $K_2=K_2'\cdot K_1$ and $1/\tau_2=k_1'$ holds true.

If the rate equation for scheme (13), $df_2(t)/dt=k_2\cdot(1-f_2(t))-k_{-2}\cdot f_2(t)$ is used with the initial condition $f_2(0)=f_2^0$ at $t=0$, integration yields:

$$f_2(t)-f_2^0=\left(f_2-f_2^0\right)\cdot(1-\exp[-t/\tau_{ME}]), \tag{17}$$

where $\tau_{ME}=\tau_2=1/k_1'$ is the relaxation time of ME.

It is recalled that the overall equilibrium constant K_2 of the poration–resealing process is directly related to the (chemical) standard value of the (Legendre-) transformed Gibbs reaction energy $\Delta_r\hat{G}^{\ominus}=\hat{G}^{\ominus}(P)-\hat{G}^{\ominus}(C_1,C)$ by $K_2=\exp(-\Delta_r\hat{G}^{\ominus}/RT)$ [42], where $R=k_B\cdot N_A$ and N_A is the Avogadro constant. The molar reaction work potential $\Delta_r\hat{G}^{\ominus}$ generally comprises chemical and physical terms such as the electric polarization energy, the pore surface and edge energies, the curvature energy term, etc. [26,40].

3.3. Coupling to Maxwell–Wagner polarization

It is shown below that the field-induced relaxations of the electrooptical signals $\Delta S(t)$ start with a sigmoidal onset. It is outlined in the discussion that the first (rapid) kinetic mode $\Delta S_I(t)$ reflects membrane stretching (MS) and smoothing of undulations (SU). The second (slower) mode $\Delta S_{II}(t)$ is ultimately caused by membrane electroporation (ME). In Appendices B and C, explicit expression for the individual terms in the sum $\Delta S(t)=\Delta S_{MS}(t)+\Delta S_{SU}(t)+\Delta S_{ME}(t)$, where $\Delta S_{MS}=\Delta S_{MS}^{\ell}+\Delta S_{MS}^{g}$ are derived. The membrane stretching terms are given by:

$$\frac{\Delta S_{MS}^{\ell}(t)}{S_0}=\frac{T_\ell}{K}=\frac{3}{8}\cdot\frac{(E\cdot a)^2\cdot C_m}{K}\cdot\left(1-\frac{\tau_{pol}\cdot\exp\left(-t/\tau_{pol}\right)-\tau_m\cdot\exp(-t/\tau_m)}{\tau_{pol}-\tau_m}\right)^2 \tag{18}$$

where τ_{pol} is the time constant of the ionic membrane polarization (Eq. (A11)),

$$\frac{\Delta S_{MS}^{g}(t)}{S_0}=\frac{T_g}{K}=\frac{3a\cdot\varepsilon_0\varepsilon_w E^2}{80\cdot K}\cdot\left(1-\frac{\tau_{pol}\cdot\exp\left(-t/\tau_{pol}\right)-\tau_m\cdot\exp(-t/\tau_m)}{\tau_{pol}-\tau_m}\right) \tag{19}$$

where ε_0 is the vacuum permittivity and $\varepsilon_W\approx 80$ the dielectric constant of water at $T=293$ K.

The undulation relaxation is specified as:

$$\frac{\Delta S_{SU}(t)}{S_0}=\frac{T_g\cdot k_B T}{8\pi\kappa\cdot(\pi\kappa/4a^2+\sigma_0)}\cdot\frac{\exp(-t/\tau_{SU})}{\tau_{SU}}\cdot B(t), \tag{20}$$

where

$$B(t)=\int_0^t\exp\left(\frac{\vartheta}{\tau_{SU}}\right)\cdot\left(1-\frac{\tau_{pol}\cdot\exp\left(-\vartheta/\tau_{pol}\right)-\tau_m\cdot\exp(-\vartheta/\tau_m)}{\tau_{pol}-\tau_m}\right)d\vartheta$$

The time course of the surface increase due to membrane electroporation is given by (Eq. (A17)):

$$\frac{\Delta S_{ME}(t)}{S_0}=f_2-f_2^0=f_2^0\cdot\tau_{ME}^{-1}\cdot\exp(-t/\tau_{ME})\cdot\int_0^t\exp\left(\vartheta/\tau_{ME}+b\cdot\langle E_m^2(\vartheta)\rangle\right)d\vartheta \tag{21}$$

Note that in the case of $\tau_{pol}\ll\tau_{ME}$, the time course of $\Delta S_{ME}(t)$ simplifies to $\Delta S_{ME}(t)/S_0=f_2^0\cdot\exp(b\cdot\langle E_m^2\rangle)\cdot(1-\exp(-t/\tau_{ME}))$.

3.4. Angular position of the DPH transition moment

The absorbance dichroism permits to determine the average angle α between the optical transition moment, $\vec{\mu}$, of the membrane probes β-DPH pPC and the membrane normal $\vec{N}$ (Fig. 1) [27]. If the average angle α between the optical transition moments of the β-DPH pPC and the membrane normal is $\alpha<54.7°$, the elongation of the vesicles in the field direction causes a global turning of the membrane chromophores from originally homogeneous radial distribution away from the external field direction (Figs. 1 and 2), leading to negative absorbance dichroism [26]. At $\alpha>0$ the amplitude of the dichroism is smaller than that for $\alpha=0$. It is known that in an electric field the extinction coefficient tensor of a chromophore in the membrane may also change due to the iono-electrochromic effect or other changes of the local environment of the chromophores, leading to a finite value of ΔA^+. However, when the chemical term ΔA^+ is very small compared to the difference term $|\Delta A^-|$ we may safely neglect the difference

$(\Delta A^{\parallel}_{CH} - \Delta A^{\perp}_{CH})$ in Eq. (4). Therefore, the reduced absorbance dichroism is given by the integral [27]:

$$\frac{\Delta A}{A_0} = \frac{\Delta A^-}{A_0} = -\frac{3}{4}\cdot S_{DPH}\cdot \int_0^{\pi} \left\{1 - 3\cdot\cos^2\left[\arctan\left(p^2\cdot\tan\theta\right)\right]\right\} \cdot\sin\theta\, d\theta. \quad (22)$$

In Eq. (22), A_0 is the initial value of the absorbance at $E=0$. $S_{DPH}=\{(3\cdot\cos^2\alpha - 1)/2\}$ is the order parameter for the optical transition moments of β-DPH pPC; see, e.g., [43,44]. Here we model the optical transition moments $\vec{\mu}$ as randomly distributed in a conical surface under the semi-angle α around the membrane normal $\vec{N}$. Note, that the orientational angle α is analogous to the cone angle for the stationary orientation in the "wobbling-in-cone" model for the fluorescence of a rod-shaped molecule with the emission moment parallel to the long axis [44]. If $\vec{\mu}$ is randomly distributed in the body of the cone of angle $\alpha_{max} > \alpha_0$, the term S_{DPH} in Eq. (22) has to be replaced by:

$$S_{DPH} = \int_0^{\alpha_{max}} \frac{3\cdot\cos^2\alpha - 1}{2}\cdot\sin\alpha\, d\alpha \Big/ \int_0^{\alpha_{max}} \sin\alpha\, d\alpha \quad (23)$$

Following the notations of Straume and Litman [19], we may express α by the fractions $f_{||}$ and $f_{\perp}$ of the optical transition moments of β-DPH pPC oriented parallel ($f_{||}$) and orthogonal ($f_{||}$) to $\vec{N}$:

$$S_{DPH} = f_{||} - \frac{f_{\perp}}{2} = \frac{3\cdot f_{||} - 1}{2}, \quad (24)$$

where the mass conservation $f_{||}+f_{\perp}=1$ has been used. Note that the parameters α, α max and $f_{||}$ ($f_{\perp}$) yield similar information on the order of $\vec{\mu}$ relative to the membrane normal.

3.5. Vesicle volume changes

At low electrolyte concentration, the vesicle volume change ΔV is directly proportional to the conductivity change $\Delta\lambda$ of the solution according to $\Delta\lambda/\lambda_{max} = -\Delta V/V_0$. Here λ_{max} is the maximum conductivity for the case that all the salt ions are completely released from the vesicle interior into the solution. The relative change of the conductivity at the pulse time t_E can be related to the relative volume change at t_E by:

$$\frac{\Delta\lambda(t_E)}{\lambda_0} = \xi\cdot\frac{\Delta V(t_E)}{V_0}. \quad (25)$$

In Eq. (25), $\xi = -\lambda_{max}/\lambda_0$ is a constant, $\lambda_0 \cong \lambda_{ex}$ the initial conductivity and V_0 the initial volume [36]. The exact analytical solution for the time course of $\Delta V(t)/V_0$ due to electromechanical deformation of the vesicle is given by a special Lambert W-function [31]. However, for short pulse durations $t_E \ll \tau_V$, where τ_V is the characteristic time of the volume change, the volume reduction is proportional to t_E, but independent of the membrane bending rigidity κ [25].

4. Results

4.1. Electrooptic relaxations and conductivity data

In Fig. 3 it is seen that the turbidity modes $\Delta T^-(t)$ and $\Delta T^+(t)$ and the absorbance modes $\Delta A^-(t)$ and $\Delta A^+(t)$ reach stationary values (amplitudes), respectively, already in the time range of about 1 μs, if the field strength is $E=5$ MV m^{-1} ($t_E=10$ μs). The data refer to a vesicle suspension of low-salt content $c_{in}=c_{ex}=0.2$ mM NaCl. As seen in Fig. 4, the amplitude $\Delta T^-/T_0$ starts to decrease with increasing cholesterol content x and $|\Delta A^-/A_0|$ starts to increase at about the same threshold mole fraction $x_{thr}=0.01$, indicating the appearance of a different membrane structure. Since the chemical terms $|\Delta T^+|$ and ΔA^+ are independent of x, cholesterol apparently does not affect the extent of the changes in the environment of the optical transition moments.

For salt-filled vesicles, $c_{in}=0.5$ M NaCl, in 0.2 mM NaCl and 0.72 M sucrose solution, the electrooptical amplitudes are smaller than for vesicles in low-salt conditions. At low-salt conditions, saturation is reached at $x_{sat}=0.5$ whereas at high-salt/sucrose conditions $x_{sat}=0.2$.

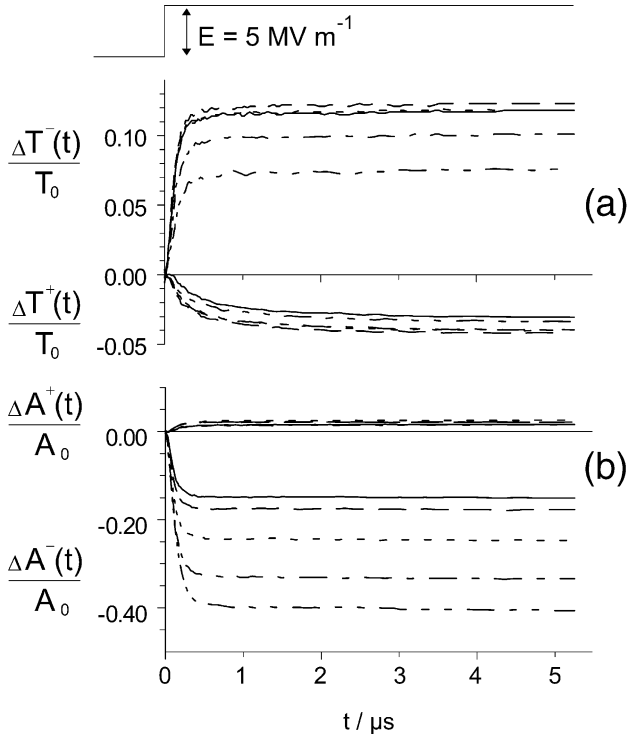

Fig. 3. Turbidity and absorbance relaxations $\Delta T^-(t)$ and $\Delta A^-(t)$ in high electric fields at low-salt conditions. (a) The difference modes $\Delta T^-/T_0=(\Delta T^{||}-\Delta T^{\perp})/(T_0)$ are positive and the plus modes $\Delta T^+/T_0=(\Delta T^{||}+2\Delta T^{\perp})/(3T_0)$ are negative, $T_0=0.20\pm0.01$, (b) the absorbance modes are $\Delta A^-/A_0=(\Delta A^{||}-\Delta A^{\perp})/(A_0)$ and $\Delta A^+/A_0=(\Delta A^{||}+2\Delta A^{\perp})/(3A_0)$, $A_0=0.24\pm0.01$, at $E=5$ MV m^{-1} and the pulse duration $t_E=10$ μs at different mole fractions x of cholesterol in the membrane: (—) no cholesterol, (– –) $x=0.04$, (- - -) $x=0.10$, (–·–) $x=0.25$ and (–··) $x=0.50$. Vesicle radius $a=50\pm3$ nm, lipid concentration 1.0 mM, [β-DPH pPC]=5.0 μM, $c_{in}=c_{ex}=0.2$ mM, $\lambda=365$ nm, $T=293$ K (20 °C).

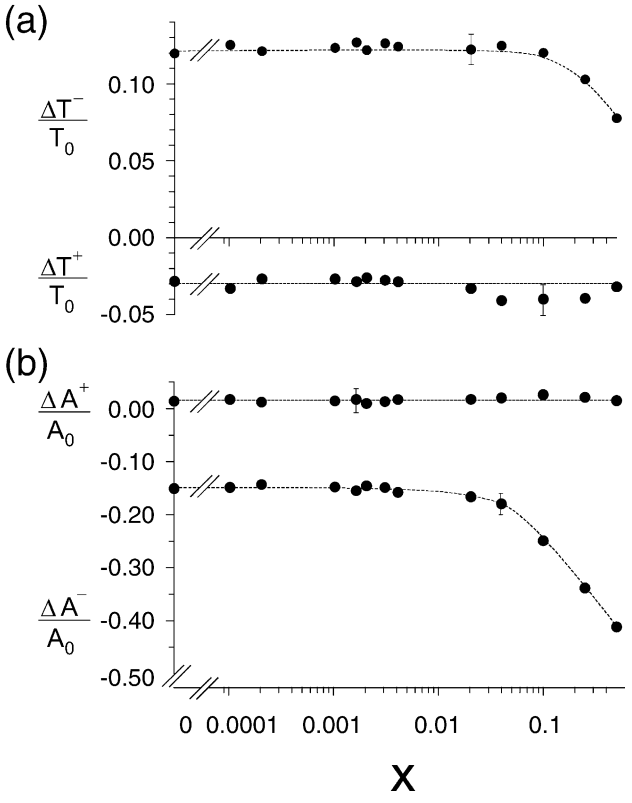

Fig. 4. The dependencies of the relaxation amplitudes on the cholesterol mole fraction x. (a) Turbidity difference mode $\Delta T^{-}/T_0=(\Delta T^{\parallel}-\Delta T^{\perp})/(T_0)$, plus mode $\Delta T^{+}/T_0=(\Delta T^{\parallel}+2\Delta T^{\perp})/(3T_0)$, (b) absorbance difference mode $\Delta A^{-}/A_0=(\Delta A^{\parallel}-\Delta A^{\perp})/(A_0)$ and plus mode $\Delta A^{+}/A_0=(\Delta A^{\parallel}+2\Delta A^{\perp})/(3A_0)$. Experimental conditions are as in the legend to Fig. 3.

4.2. Conductivity changes and volume reduction

A typical example of small ion release due to electroporation of salt-filled vesicles is shown in Fig. 5. The volume reduction $\Delta V/V_0$ is calculated with Eq. (25) from the relative conductivity change $\Delta\lambda/\lambda_0$, caused by the field pulse and measured 5 min after the pulses for two typical field strengths. The changes start to become smaller with increasing cholesterol content at about $x=0.01$, being larger at the higher field strength by factor of about 5 compared to the lower field strength. Visual inspection shows that the trend in the conductivity term $\Delta\lambda/\lambda_0$ is reflected in the volume term $\Delta V/V_0$.

5. Data analysis and discussion

5.1. Vesicle elongation parameters

In Fig. 6(a), it is seen that the vesicle deformation parameter p at the typical field strength $E=5$ MV m^{-1}, calculated from the turbidity modes ΔT^{-} and ΔT^{+} as outlined in [35], starts to decrease with increasing cholesterol content of the membrane at the apparent threshold $x_{thr}=0.06$. For $x>x_{thr}$, the deformability of the vesicles is lower both for low-salt conditions and for salt-filled vesicles. In the range $0\le x\le 0.05$, it is mainly Δp_v that contributes to p, see Eq. (8). At $E=5$ MV m^{-1}, $\Delta p_s\le 0.057\pm0.005$ and at $E=7$ MV m^{-1}, $\Delta p_s=0.117\pm0.005$. Clearly $|\Delta V/V_0|$ and thus Δp_s decreases with increasing x (Fig. 5). At low salt conditions Δp_v is experimentally not accessible. We therefore approximate Δp_v (low salt) $\approx \Delta p_v$ (high salt) for calculation of ΔS. Note that for salt-filled vesicles and $E\le 5$ MV m^{-1}, $\Delta V/V_0\approx 0$ (Fig. 5). Therefore, for the case $\Delta p_s=0$, Eq. (8) reduces to $p=1+\Delta p_v$.

5.2. Membrane refractive index

The calculation of p requires knowledge of the refractive index n_m of the membrane. In aqueous solution, the membrane refractive index at the wavelength $\lambda=366$ nm and at the temperature $T=293$ K is $n_m=1.507$ [45]. The analysis of the optical density spectrum $OD_0(V,\lambda)=T_0(\lambda)$ (in the absence of the field pulse) yields the membrane refractive index for both the low-salt conditions n_m (low salt) $=1.507\pm0.002$ and for the salt-filled vesicles n_m (high salt) $=1.525\pm0.002$. For the low-salt condition $c=0.2$ mM NaCl we have: $n_{in}=n_{ex}=n_{water}=1.347$, for salt-filled vesicles ($c_{in}=0.5$ M NaCl): $n_{in}(0.5\text{ M})=1.376$ and for 0.72 M sucrose n_{ex} (0.72 M) $=1.382$.

5.3. The mode ΔT^{+} reflects water entrance

It is recalled that the field pulse-induced change ΔT^{+} (Fig. 3) is negative, which is consistent with a field-induced decrease in the average effective index of the membrane, defined by [46]:

$$n_m(E) = (1-\Delta f_W)\cdot n_m(0) + \Delta f_W \cdot n_W(E) \qquad (26)$$

In Eq. (26), $\Delta f_W=f_W(E)-f_W(0)$ is the field-induced change in the volume fraction f_W of water in the membrane.

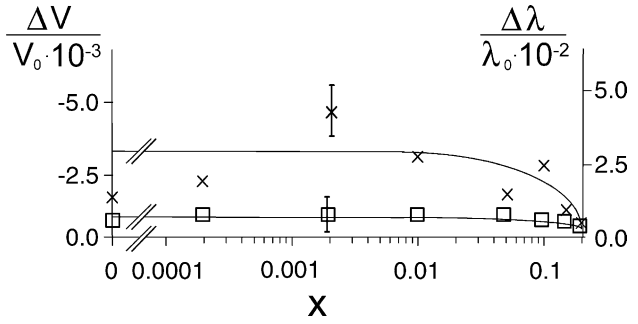

Fig. 5. Relative volume change $\Delta V/V_0$ of the vesicles filled with 0.5 M NaCl in 0.72 M sucrose and 0.2 mM NaCl solution (external medium) as a function (of the logarithm) of the mole fraction x of cholesterol in the membrane, calculated with Eq. (25) and $\xi=-9.5$ from the relative conductivity increase $\Delta\lambda/\lambda_0$ of the suspension at the end of the pulse of duration $t_E=10$ μs and field strength $E=5.0$ MV m^{-1} (□) and $E=7.0$ MV m^{-1} (×), respectively. The solid lines are drawn to illustrate the trends in the dependencies of $\Delta\lambda/\lambda_0$ and $\Delta V/V_0$, respectively. The initial conductivity is $\lambda_0=4.1$ μS cm^{-1}; other experimental conditions are as in the legend to Fig. 3.

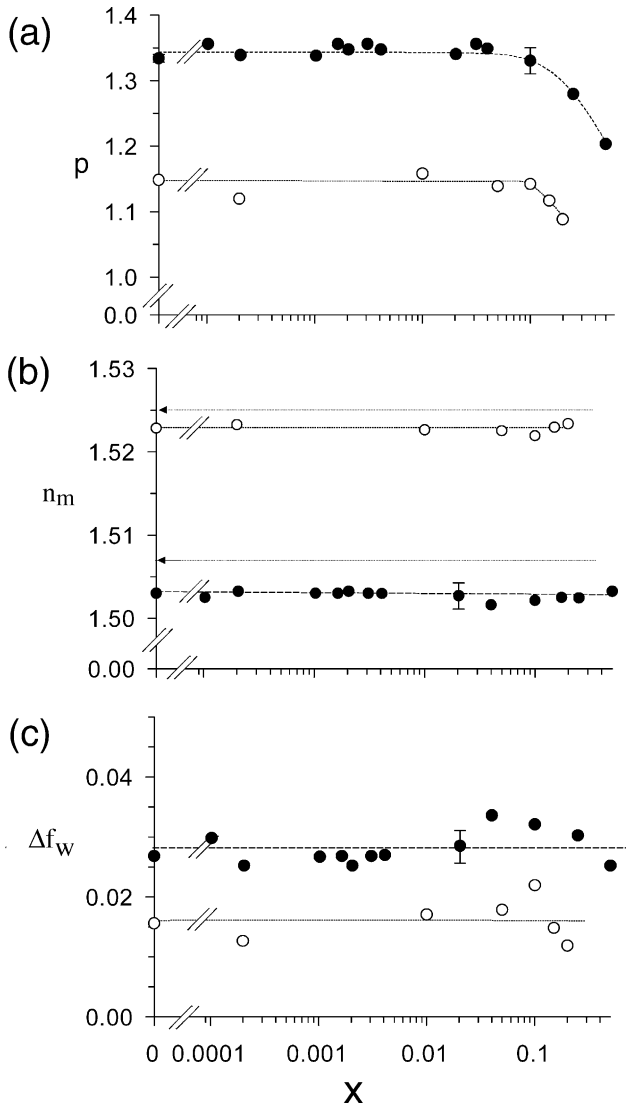

Fig. 6. Logarithmic dependencies of p, n_m and Δf_W on the mole fraction x of cholesterol. (a) The axis ratio $p=c/b$ of an elongated vesicle (Fig. 2), (b) the membrane refractive index nm and (c) the increase in the volume fraction of membrane water Δf_W at $t_E=10$ μs and $E=5$ MV m^{-1}, calculated from the modes $\Delta T^-/T_0$ and $\Delta T^+/T_0$. The arrow (←) in (b) indicates n_m at $E=0$. In (a), (b) and (c): (●) refers to vesicles with $c_{ex}=c_{in}=0.2$ mM NaCl and (○) refers to vesicles filled with 0.5 M NaCl in 0.72 M sucrose and 0.2 mM NaCl solution (external medium). Other experimental conditions are as in the legend to Fig. 3.

Obviously, $f_W(E)$ and $n_m(E)$ refer to the presence of the field E and $f_W(0)$ and $n_m(0)$ are the values at $E=0$. At $E=5$ MV m^{-1}, $n_m(E)=1.502$ is about 0.3% smaller than $n_m(0)=1.507$ for the low-salt condition of $c_{in}=c_{ex}=0.2$ mM NaCl. For salt-filled vesicles $n_m(E)=1.522$ is about 0.2% smaller than $n_m(0)=1.525$.

Note that Δf_W, as average along the membrane normal, is different for the low-salt conditions $\Delta f_W(E$, low salt$)=0.027$ compared to the high-salt/sucrose conditions $\Delta f_W(E$, high salt$)=0.015$. Both values appear to be independent of the cholesterol content; see Fig. 6(c).

Actually, Δf_W in the head group region is larger than in the hydrocarbon part of the lipid membrane. If the increase in the water content is related solely to the two lipid head group layers of thickness $d_h=0.74$ nm [47], the water content in the layers is increased by $\Delta f_w \cdot d/(2\cdot d_h)=0.05$ and 0.09, for the salt-filled and low-salt vesicles, respectively. This is comparatively smaller than the water volume fraction of about 0.2 (12 water molecules per lipid molecule) in the head group region of fully hydrated egg-yolk phosphatidylcholine bilayer, derived from X-ray diffraction at $E=0$ [48]. The conclusion that Δf_W refers dominantly to water entrance into the head-group layers is also in line with ^{31}P NMR data, showing that up to 70% of the phospholipids in the electro-permeabilized plasma membrane appear to have an altered organization of the polar heads [49].

In any case, at low-salt concentration the field-induced water entrance is larger than at the dehydrating conditions of high salt concentration (0.5 M NaCl) and high sucrose content (0.72 M). It should be noted that the volume reduction $\Delta V/V_0$ only partially rationalizes the large value of ΔT^+. A part of ΔT^+ may result from a field-induced change $\Delta d=d(E)-d$ in the membrane thickness d, where $d(E)$ refers to the presence of the field and $\Delta d/d=-\Delta S_{MS}/S_0$. Using Eq. (10), $K=0.2$ N m^{-1} [12] and the components T_g and T_ℓ of the stress tensors at $E=5$ MV m^{-1}, we find that $\Delta d/d=-1.4\cdot 10^{-3}$. This is too small to account for the actual value $\Delta T^+/T_0=0.04$ (Fig. 3).

5.4. The field-induced surface area changes ΔS(t)

It is recalled that the calculated rate-limiting process for the onset of the relaxation $\Delta S(t)=\Delta S_{MS}(t)+\Delta S_{SU}(t)+\Delta S_{ME}(t)$ of the membrane surface is the ionic membrane polarization. See Appendices B and C, where Eq. (A11) is used to calculate the polarization time constant τ_{pol}.

For the low-salt condition of $c_{in}=c_{ex}=0.2$ mM NaCl, where $\lambda_{in}=\lambda_{ex}=3.8$ mS/m, we find $\tau_{pol}=0.11$ μs. For salt-filled vesicles, where $\lambda_{in}=1.57$ S/m refers to 0.5 M NaCl solution and $\lambda_{ex}=0.41$ mS/m to 0.2 mM NaCl and 0.72 M sucrose, we obtain $\tau_{pol}=0.35$ μs. Obviously, the dehydrating conditions of high-salt and high-sucrose content slows down the ionic polarization process.

Because the time constants τ_{SU} and τ_{pol} are approximately equal, the field-induced smoothing of undulations appears to occur as fast as the polarization process; see Eq. (11). In any case, because $\tau_{MS} \ll \tau_{SU}$, see Eq. (9), the membrane stretching is rapidly coupled to the slower polarization process.

5.4.1. Normal mode parameters

As outlined above, the two main contributions of the experimental curve $\Delta S(t)=\Delta S_I(t)+\Delta S_{II}(t)$ are the very rapid membrane stretching ($\Delta S_I(t)$) and the slower smoothing of undulations ($\Delta S_{II}(t)$). Since $\tau_{MS} \ll \tau_{SU}$, the time constant of

the first phase is given by $\tau_I=\tau_{SU}$ and the amplitude ΔS_I by [38]:

$$\frac{\Delta S_I}{S_0}=\frac{3}{8}\cdot\frac{(E\cdot a)^2\cdot C_m}{K}+\frac{3a\cdot\varepsilon_0\varepsilon_w E^2}{80\cdot K}\cdot\left(1+\frac{k_B T}{8\pi\kappa\cdot(\pi\kappa/4a^2+\sigma_0)}\right) \quad (27)$$

It is found that the experimental amplitude ΔS_I compares well with that calculated with Eq. (27). The explicit time courses of the polarization-controlled processes MS and SU are described by the Eqs. (18)–(20). The slower mode ΔS_{II} is similar to that of membrane electroporation [35]. Therefore we identify $\tau_{II}=\tau_{ME}$. The exact time course of $\Delta S_{II}(t)=\Delta S_{ME}(t)$ is described by Eq. (21). It is interesting that at the low-salt condition of $c_{in}=c_{ex}=0.2$ mM NaCl, the time constant $\tau_I=\tau_{SU}$ is independent of the cholesterol content (Fig. 7(a), left panel), whereas both the large amplitude ΔS_I and the small amplitude ΔS_{II} start to decrease at about $x=0.07$ (Fig. 7(b), left panel). At the same low-salt condition, the electroporation-associated time constant $\tau_{II}=\tau_{ME}$ increases with x (Fig. 7(a), left panel). Since at the low-salt condition $\Delta S_{II}<\Delta S_I$, membrane stretching and smoothing are much larger than the surface area increase due to membrane electroporation.

For salt-filled vesicles, the amplitude $\Delta S_{II}=\Delta S_{ME}$ of membrane electroporation is larger than $\Delta S_I=\Delta S_{SU}+\Delta S_{MS}$ (Fig. 7(b), right panel). The surface change is thus dominated by $\Delta S_{ME}(t)$. The sigmoid onset of $\Delta S(t)$ reflects that ME is rate limited by the initial membrane charging. At $x=0.1$, both ΔS_{ME} and ΔS_{SU} decrease with x. Summing up, increasing cholesterol content decreases both the rates and extents of the field-induced membrane processes.

5.5. Membrane compressibility and bending rigidity

Since cholesterol is known to affect the membrane compressibility K and the bending rigidity κ, the dependencies $K(x)$, $\kappa(x)$ and the initial lateral membrane tension σ_0 are calculated from the amplitude $\Delta S_I=\Delta S_{SU}+\Delta S_{MS}$ with Eqs. (10) and (12), respectively. At the low-salt condition, the membrane compressibility is in the range $0.2\le K/(\mathrm{N\ m^{-1}})\le 0.6$ and the bending rigidity in the range $2.9\le\kappa/10^{-20}\ \mathrm{J}\le 5.8$ for the cholesterol fraction $0\le x\le 0.5$ (Fig. 8), consistent with reference data [10]. The tension $\sigma_0=2.10^{-4}\ \mathrm{mNm^{-1}}$ is found to be independent of x.

For the high-salt conditions, the parameters are in the ranges $0.9\le\kappa/10^{-19}\ \mathrm{J}\le 3.3$ and $0.55\le K/\mathrm{N\ m^{-1}}\le 6.0$ for the range $0\le x\le 0.2$ and $\sigma_0=1.10^{-4}\ \mathrm{mNm^{-1}}$, respectively (Fig. 8). These K values are in the range of those ($K\le 0.7$ N m^{-1}) given by Needham and Nunn [10]. The elastic parameters K, κ and σ_0 are dramatically increased in the presence of 0.72 M sucrose and 0.5 M NaCl compared to the low-salt conditions. As a consequence, the amplitude of the first phase ΔS_I becomes tenfold smaller than $\Delta S_{II}=\Delta S_{ME}$ and the overall $\Delta S/S_0$ decreases (Fig. 7(b), right panel).

The analysis of $\Delta S_{ME}(t)$ at both $x=0.2$ and $x=0$ (Fig. 9(a) and (b)) with Eqs. (18)–(21), respectively, yields the

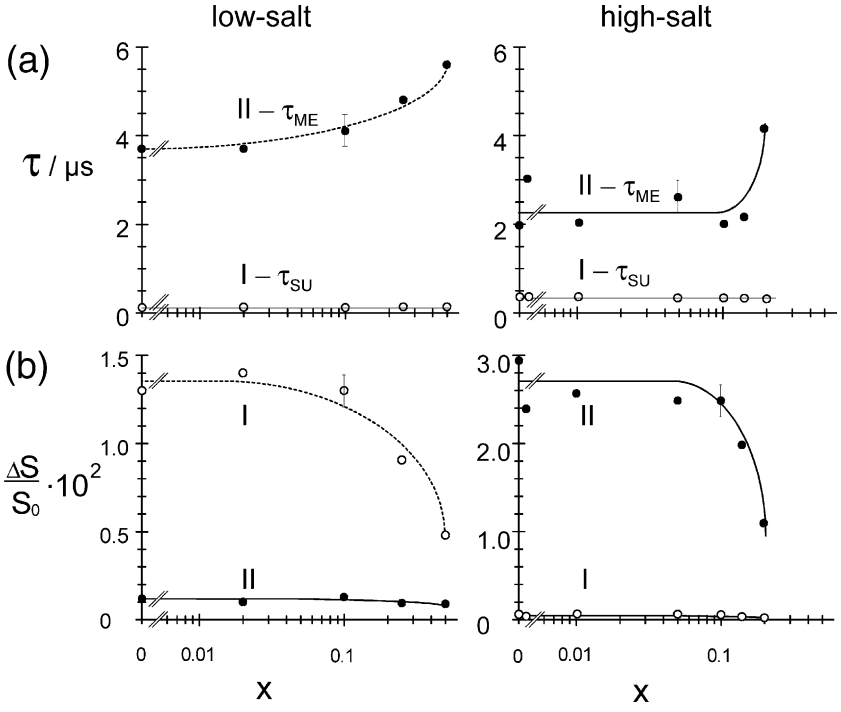

Fig. 7. Dependence of (a) the time constant τ and of (b) the amplitude $\Delta S/S_0$ of the rapid (○) and the slower (●) modes on the mole fraction x of cholesterol for the low-salt conditions $c_{ex}=c_{in}=0.2$ mM NaCl (left column) and for the salt-filled vesicles with $c_{in}=0.5$ M NaCl, $c_{ex}=0.2$ mM NaCl and 0.72 M sucrose solution (left column), respectively. Rectangular electric pulse of $E=5.0$ MV m^{-1} and $t_E=10$ µs pulse duration. Other experimental conditions are as in the legend to Fig. 3.

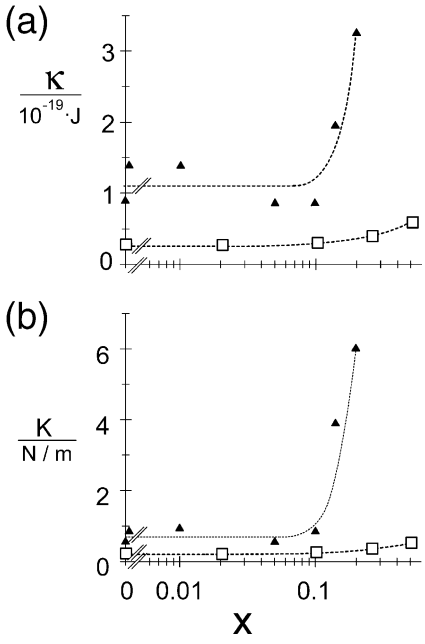

Fig. 8. The membrane bending rigidity κ (a) and the stretching modulus K (b) of the salt-filled vesicles (▲) and of the vesicles with $c_{ex}=c_{in}=0.2$ mM NaCl (□) as a function of the mole fraction x of cholesterol. Other experimental conditions are as in the legend to Fig. 7.

same electroporation parameter $b=2.4\cdot10^{-13}$ m^2 V^{-2}, see Eq. (A19). However, the electroporation time constants are different: $\tau_{II}=\tau_{ME}=4.35$ μs at $x=0.2$ and $\tau_{ME}=2.0$ μs at $x=0$.

Interestingly, ΔS_{ME} and τ_{ME}^{-1} for the high-salt condition are about twofold larger than ΔS_{ME} and τ_{ME}^{-1} for $c_{in}=c_{ex}$, respectively (Fig. 7). This experimental fact is in line with the physical–chemical electroporation theory, rationalizing the increase in extent and rate of ME in salt-filled vesicles by an increase in the electrostatic part of the elastic parameters and the membrane spontaneous curvature due to the transmembrane salt gradient [40]. The larger values of K, κ and σ_0 of salt-filled vesicles are also consistent with major dehydration of the membrane in 0.72 M sucrose solution. The stronger dependence of K and κ on x can be rationalized by the more compact packing of the lipid molecules in the membrane of salt-filled vesicles. The decrease in $\Delta S_{ME}/S_0$ and $\tau_{ME}^{-1}=\tau_{||}^{-1}$ with increasing x is in line with the inhibitory effect of cholesterol on ME [9]. In summary, sucrose and salt gradient across the membrane favor ME but decrease membrane stretching (MS) and undulations (SU).

Membrane cholesterol decreases not only MS and SU, but also ME, leading to a decrease in the degree of electroelongation of vesicles.

5.6. Radius of electropore

Using the identity $\Delta S_{II}(t)=\Delta S_{ME}(t)=f_2(t)\cdot S_0$, Eq. (17) is applied to the data in Fig. 9. The amplitude analysis uses the identity $f_2=K_2$; see Eq. (16) for $f_2 \ll 1$. Applying Eqs. (A18) and (A19), we obtain the mean pore radius $\bar{r}_p=[b/\pi\cdot\varepsilon_0\cdot(\varepsilon_w-\varepsilon_L)\cdot d/(2k_BT)]^{1/2}=0.9\pm0.1$ nm from the fit parameter $b=2.4\cdot10^{-13}$ m^2 V^{-2}. Obviously, the number of pores per vesicle is given by [50]:

$$N_p^{ves}=\frac{4\cdot a^2}{\bar{r}_p^2}\cdot\frac{\Delta S_{ME}}{S_0} \quad (28)$$

For the range $0\le x\le0.2$ we have $31\ge N_p^{ves}\ge15$. The mean pore radius calculated from $\Delta S(t)/S_0$ is the same as $\bar{r}_p=0.9\pm0.1$ nm, derived from previous conductometric data of PC/PG-vesicles (PC/PG=1:1) of radius $a=50\pm3$ nm at $E=1$ MV m^{-1} and in the (long) time range $5\le t_E/\text{ms}\le60$ [31,36]. For lecithin (20%) vesicles of radius $a=90$ nm in the range $1\le E/\text{MV m}^{-1}\le7.5$ and at $t_E=10$ μs [35], the analysis of the release of Na^+- and Cl^--ions through the pores yields a smaller radius: $\bar{r}_p=0.56\pm0.05$ nm.

The turbidity (T_0) in non-polarized light show that cholesterol does not affect the refractive index of the membrane (data not shown). Therefore x does not change the difference $(\varepsilon_w-\varepsilon_L)$ and, consequently, the pore radius $\bar{r}_p=[b/\pi\cdot\varepsilon_0\cdot(\varepsilon_w-\varepsilon_L)\cdot d/(2k_BT)]^{1/2}$. The quantity $\Delta S_{ME}/S_0$ and $\tau_{ME}^{-1}=\tau_{II}^{-1}$ depend on x dominantly through the line tension of the pore edge, the surface tension of the membrane and the packing density of lipid molecules [40].

5.7. Fraction of pores and water content of the membrane

The field induced relative increase in the membrane water content $\Delta f_W=0.016$, Fig. 6(c), is about tenfold larger than the electroporative increase in the membrane volume: $\Delta V_{ME}^m/V_0^m=d\cdot\Delta S_{ME}/(d\cdot S_0)=0.0029$ for salt-filled vesicles. For low-salt vesicles, we have $\Delta f_W=0.028$ and $\Delta V_{ME}^m/V_o^m=0.0012$ (Fig. 7(b) at $x=0$). Since $\Delta f_W \gg \Delta V_{ME}^m/V_0^m$, the membrane electropores cannot be solely responsible for Δf_W. Rather, besides the electropores, water appears to enter into the head group region of the lipid bilayer due to the global Maxwell stress. In addition, the induced membrane

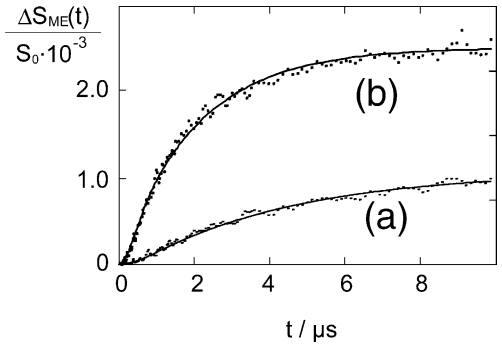

Fig. 9. Surface area relaxations. The relative increase $\Delta S_{ME}(t)/S_0$ in the membrane surface areas of lipid vesicles at $E=5.0$ MV m^{-1} as a function of time: (a), at the mole fraction $x=0.2$ of cholesterol and (b), at $x=0$. The solid line is the theoretical simulation of $\Delta S_{ME}(t)/S_0$ using Eq. (21) of the text. Salt-filled vesicles (0.5 M NaCl) in 0.2 mM NaCl and 0.72 M sucrose solution (external medium). Other experimental conditions are as in the legend to Fig. 3.

field causes orientational changes of the lipid head groups in the transmembrane field [51]. This suggestion is consistent with the decrease in the refractive index n_m as measured with the turbidity plus mode $\Delta T^+/T_0$.

5.8. Position of reporter lipids in the membrane

It is recalled that cholesterol affects the amplitudes of the turbidity (ΔT^-) and the absorbance (ΔA^-) modes, respectively, in a different manner (Fig. 4), but both ΔT^- and ΔA^- indicate electroporative vesicle deformation. However, if the presence of cholesterol solely decreases $\Delta S/S_0$ and thus the degree p of vesicle elongation, the absolute values $|\Delta T^-|$ and $|\Delta A^-|$ should decrease nearly parallel with increasing cholesterol content x. However, $|\Delta T^-|$ decreases whereas $|\Delta A^-|$ increases with increasing x (Fig. 4). The numerical analysis for the mantled ellipsoids shows that p decreases with increasing x. Analysis of ΔA^- with Eq. (22) at constant angle α suggests that p increases with increasing x. Apparently, ΔA^- reflects not only vesicle elongation, but also a decrease in the average angle α between the optical transition moment of β-DPH pPC and the membrane normal (Fig. 1).

5.9. Membrane order and lipid alignments

5.9.1. Cholesterol orders the β-DPH pPC molecule

Substitution of the axis ratio p, obtained from the stationary values of the turbidity relaxations ΔT^- and ΔT^+ (Fig. 3(a)), into Eq. (22) and analysis of ΔA (Fig. 3(b)) shows that the average angle α is a function of x (Fig. 10(a)). The data suggest that at $x=0$, $\alpha=45°$ at $c_{ex}=c_{in}=0.2$ mM NaCl and $\alpha=38°$ for vesicles filled with 0.5 M NaCl and suspended in 0.72 M sucrose and 0.2 mM NaCl solution. If the chromophores are randomly distributed in the cone body of the semi-angle α_{max}, Eq. (23), the maximum angles are $\alpha_{max}=69°$ and $\alpha_{max}=56°$ for low-salt and salt-filled vesicles, respectively. In terms of $f_{||}$ and $f_{\perp}$, Eq. (24), at $x=0$ the fraction of β-DPH pPC parallel to the membrane normal $\vec{N}$ is $f_{||}=0.5$ for low-salt vesicles and $f_{||}=0.62$ for salt-filled vesicles, respectively. At $x=0.5$, $f_{||}=0.995$ for low-salt vesicles at $x=0.2$ and $f_{||}=1$ for salt-filled vesicles. The fraction $f_{||}=0.5$ of β-DPH pPC in low-salt vesicles at $x=0$ compares well with $f_{||}=0.45$ at $x=0$ of 1,6-diphenyl-1,3,5-hexatriene (DPH) in dioleoylphosphatidylcholine (DOPC) vesicles ($T=37$ °C), determined from the analysis of the fluorescence anisotropy decay [19]. The fact that $f_{||}=0.5$ of β-DPH pPC is larger than $f_{||}=0.45$ of DPH is rationalized by the covalent coupling of DPH in the β-DPH pPC molecule. Obviously, there is less rotational freedom for the β-DPH pPC molecule than for the free DPH in the membrane.

With increasing x (Fig. 10(a)), the angle α of the DPH-chromophore relative to $\vec{N}$ becomes smaller, suggesting that the DPH lipids are more aligned along the membrane normal. This is in line with the observation that cholesterol

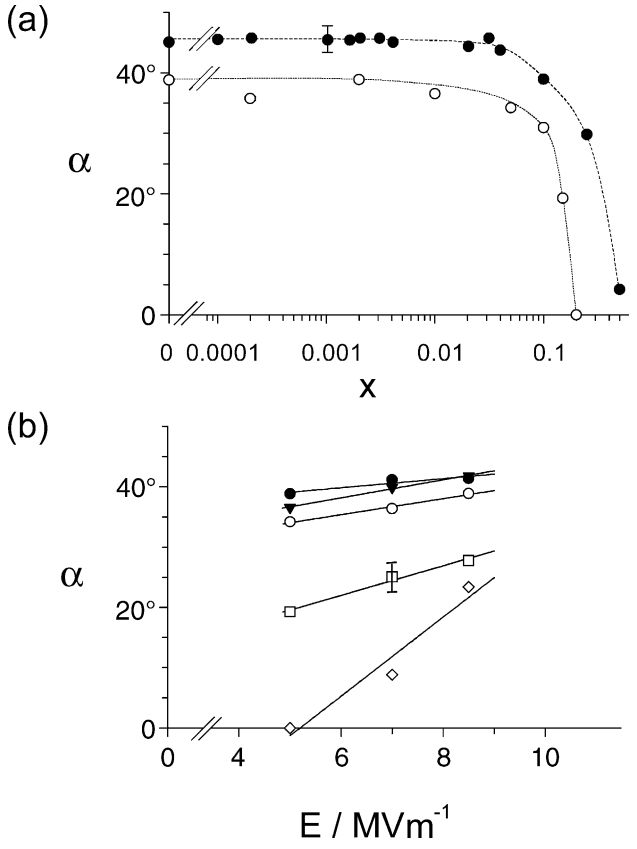

Fig. 10. The stationary value of the average angle α of the optical transition moment of the chromophore β-DPH pPC relative to the membrane normal (Fig. 1). (a) Low-salt conditions (●) $c_{ex}=c_{in}=0.2$ mM NaCl, and (○) salt-filled vesicles (0.5 M NaCl) in 0.2 mM NaCl and 0.72 M sucrose solution (external medium), as a function of the mole fraction x of cholesterol at $E=5$ MV m^{-1} and $t_E=10$ μs. (b) α as a function of the field strength E for different mole fractions x of cholesterol: (●) $x=0$, (▼) $x=0.01$, (○) $x=0.05$, (□) $x=0.15$ and (◊) $x=0.20$ for the salt-filled vesicles (0.5 M NaCl) in 0.2 mM NaCl and 0.72 M sucrose solution (external medium). Other experimental conditions are as in the legend to Fig. 3.

hinders the conformational flexibility of the upper portions of the lipid acyl chains [10,52–54]. The decrease of α with increasing x is also consistent with X-ray diffraction data and dielectric capacitance data, suggesting that cholesterol decreases the depth of water penetration into the bilayer [55,56]. Therefore there is less space for β-DPH pPC to deviate from the $\vec{N}$ direction [44].

If there are raft-like domains of cholesterol in the vesicle membrane, the cholesterol would affect the position of β-DPH pPC molecules only at the boundaries of the rafts but not in the rest of the membrane [57]. Therefore, cholesterol rafts cannot cause the alignment of the practically all the evenly distributed DPH-chromophores along the membrane normal. Note that $f_{||}=0.995$ ($x=0.5$) for low-salt vesicles and $f_{||}=1.0$ ($x=0.2$) for salt-filled vesicles. So we can safely exclude the dominance of pure cholesterol rafts.

5.9.2. Order by sucrose

In the salt-filled vesicles (0.5 M NaCl) in 0.72 M sucrose solution, the alignment of β-DPH pPC parallel to the

membrane normal is more pronounced than in vesicles with $c_{ex}=c_{in}=0.2$ mM NaCl , Fig. 10(a), consistent with the dehydration of the lipid membrane in the presence of sucrose. Dehydration solely by 0.5 M NaCl is less probable, because 1 M NaCl electrolyte produces little or no changes in the bilayer structure [48]. Various methods show that dehydration increases the bilayer thickness and decreases the area per lipid molecule, leading to a larger lipid packing density. This, in turn, leads to less free space for the β-DPH pPC motion. Dehydration and increase in the packing density of the lipids correlate well with the larger refractive index nm and the smaller content of water in the membrane of the salt-filled vesicles (Fig. 6(b),(c)).

5.9.3. Electric fields change the alignment of β-DPH pPC

For the salt-filled vesicles at $x=0$, the angle α weakly increases in the range $38°\leq\alpha\leq41°$ with increasing field strength in the range $5\leq E/\mathrm{MV\ m^{-1}}\leq8.5$ (Fig. 10(b)). At $x=0.2$, the decrease of the alignment of the optical transition moments of β-DPH pPC (parallel to $\vec{N}$) is stronger: $0°\leq\alpha\leq23°$ in the range $5\leq E/\mathrm{MV\ m^{-1}}\leq8.5$. If the displacement of β-DPH pPC in the field is solely due to the field-induced membrane thinning, the increase in α should reflect an unreasonably large change in the membrane surface area $\Delta S/S_0\approx-\ \Delta d/d=-\ (\cos(8.5°)-\cos(5°))=0.033$ for $x=0$ and $\Delta S/S_0=0.079$ for $x=0.2$. On the contrary, the increase in α is rationalized by the rotational displacement of the chromophore residue caused by the alignment of the dipolar head groups in the field direction [27]. Since the conformation of the β-DPH pPC lipids is similar to that of non-labeled lipids, the field-induced alignment of β-DPH pPC is concomitant with an alignment of all other lipid molecules of the membrane.

6. Conclusion

The electrooptic and conductometric relaxation data in high electric fields indicate that the electro-deformation of vesicles is associated with three different processes: membrane electroporation (ME), smoothing of membrane undulations (SU) and membrane stretching (MS). The small electropores of the mean radius of $\bar{r}_p=0.9\pm0.1$ nm lead to electrolyte efflux from the vesicle interior, concomitant with vesicle elongation.

In the presence of cholesterol, both ME and the membrane surface area increase due to MS and SU are reduced. Additionally, cholesterol increases the alignment of the β-DPH pPC lipid molecules parallel to the membrane normal and thereby increases the lipid packing density. Similarly to cholesterol, the presence of 0.72 M sucrose in the medium increases the order of the β-DPH pPC molecules in the membrane, decreasing the degree of vesicle elongation in an electric field. The ordering effect of sucrose is in line with the larger values of the membrane refractive index of salt-filled vesicles. In an electric field pulse, the refractive index is smaller due to the increase in the volume fraction of membrane water. An electric field can transiently decrease the alignment of β-DPH pPC molecules along the membrane normal. Surprisingly, the electric field leads to water entrance not only locally to form the electropores, but also globally into the lipid head group layers. Consistent with the previous results of membrane electroporation in ionic strength gradients [40], extent and rate of ME are (nearly twofold) larger in salt-filled vesicles than in low-salt vesicles.

Acknowledgments

We thank the Deutsche Forschungsgemeinschaft for grant Ne 227/9, the ministry MSWF of the land NRW for grant ELMINOS, the Fonds Chemie and the EU, Brussels, for grant QLK3-CT-1999-00484 to E. Neumann.

Appendix A. Lambert–Beer's law

We use Lambert–Beer's law for the absorbance:

$$A=\ell\cdot\sum_i\varepsilon_i\cdot c_i, \tag{A1}$$

where ε_i is the molar extinction tensor and c_i the concentration of species i, ℓ is the optical path way.

For optically anisotropic ellipsoidal particles, with two components $\varepsilon_{\parallel,i}$ and $\varepsilon_{\perp,i}$, the conventional extinction coefficient is the orientational mean: $\bar{\varepsilon}_i=(\varepsilon_{\parallel,i}+2\varepsilon_{\perp,i})/3$. In polarized light it is practical to subdivide the field-induced change $\mathrm{d}A$ into two (independent) contributions. The total differential [30]

$$\mathrm{d}A=\ell\cdot\left(\sum_i\varepsilon_i\cdot\mathrm{d}c_i+\sum_i c_i\cdot\mathrm{d}\varepsilon_i\right), \tag{A2}$$

contains the chemical concentration changes $\mathrm{d}A_{CH}=\ell\cdot\sum_i\varepsilon_i\cdot\mathrm{d}c_i$ and the orientational changes $\mathrm{d}A_{OR}=\ell\cdot\sum_i c_i\cdot\mathrm{d}\varepsilon_i$, such that the integral change is specified as:

$$\Delta A=\Delta A_{CH}+\Delta A_{OR}, \tag{A3}$$

See Eq. (2) of the main text. For dilute solutions of light scattering particles the forward-light scattering term, expressed as turbidity T obeys a concentration dependence in a similar way as Lambert–Beer's law for the absorbance. Hence, analogous to Eq. (A1), the turbidity is given by:

$$T=\ell\cdot\sum_i y_i\cdot c_i, \tag{A4}$$

where y_i is a kind of the molar scattering tensor of species i. Assuming that the scattering centers are independent, analogous to Eq. (A3), we may write:

$$\Delta T=\Delta T_{CH}+\Delta T_{OR}, \tag{A5}$$

If, in addition, the light extinction centers leading to the absorbance A are independent of the light scattering centers leading to the turbidity T, then the approximations

$$\mathrm{OD} = A + T \tag{A6}$$

and

$$\Delta\mathrm{OD} = \Delta A + \Delta T, \tag{A7}$$

are justified.

Appendix B. Global and local Maxwell membrane tensions

The global Maxwell stress is dependent on the positional angle θ, see Fig. 2 of the main text. The θ-average $\langle T_g^{\theta}\rangle$ of the global Maxwell tension T_g is given by [31]:

$$T_g = \langle T_g^{\theta}\rangle = \frac{3a}{80}\left\{\varepsilon_0\varepsilon_w E^2 \cdot f_\lambda^2 - \frac{64\kappa\cdot(p-1)}{3a^3}\right\} \tag{A8}$$

where f_λ is the conductivity factor. At $\lambda_{in} \gg \lambda_{ex}$, the approximation $f_\lambda = \lambda_m \cdot a/(2\cdot\lambda_{ex}\cdot d)$ holds, where λ_m, λ_{ex} and λ_{in} are the conductivities of the vesicle membrane, the bulk solution and the vesicle interior, respectively [35]. Note, the derivation of Eq. (A8) contains the Laplace expression $T_g = a\cdot P_g/4$, referring to the two water–lipid interfaces of the lipid membrane [38]. The global average pressure is given by $P_g = 3a/20\cdot\left\{\varepsilon_0\varepsilon_w E^2 \cdot f_\lambda^2 - 64\kappa\cdot(p-1)/3a^3\right\}$.

The θ-average of the local Maxwell stress T_ℓ across the membrane is given by [9]:

$$T_\ell = \frac{C_m\cdot\langle\Delta\varphi^2\rangle}{2}, \tag{A9}$$

where $C_m = 0.5\ \mu\mathrm{F\ cm^{-2}}$ is the specific membrane capacitance. The term $\langle\Delta\varphi^2\rangle$ is the θ-average of the induced (squared) transmembrane potential difference in the direction of the membrane normal according to [35]:

$$\langle\Delta\varphi^2\rangle = (1.5\cdot a\cdot E\cdot f_\lambda)^2\cdot\int_0^{\pi/2}\cos^2\theta\cdot\sin\theta\,\mathrm{d}\theta, \tag{A10}$$

where θ is the positional angle relative to the field strength vector $\vec{E}$ (Fig. 2). For $f_\lambda \approx 1$, the approximation $\langle\Delta\varphi^2\rangle = 3\cdot a^2\cdot E^2/4$ applies [35].

Appendix C. Time constant τ_{pol} of the ionic membrane polarization

The time resolution of the modes $\Delta S_{MS}(t)$, $\Delta S_{SU}(t)$ and $\Delta S_{ME}(t)$ is technically limited by the spark gap discharge time controlling the switch-on of the electric field and by the time constant τ_{pol} of the ionic membrane polarization. The machine time of the field-jump relaxation spectrometer is $\tau_m \leq 0.07\ \mu\mathrm{s}$. The characteristic time of the membrane ionic polarization is given by [58]:

$$\tau_{pol} \approx a\cdot C_m\cdot\left(\lambda_{in}^{-1} + \lambda_{ex}^{-1}/2\right) \tag{A11}$$

In the case of in $\lambda_{in} = \lambda_{ex} = 3.8\ \mathrm{mS\ m^{-1}}$, Eq. (A11) yields $\tau_{pol} = 0.11\ \mu\mathrm{s}$, which is comparable with $\tau_m = 0.07\ \mu\mathrm{s}$. Therefore, the increase in the field strength E_m of the membrane of thickness d can be formulated along the lines given by Eigen and DeMayer [59]. Here, the differential equation for $E_m(t)$ is specified as:

$$\frac{\mathrm{d}E_m}{\mathrm{d}t} + \frac{E_m}{\tau_{pol}} = \frac{1.5\cdot E\cdot a\cdot f_\lambda\cdot|\cos\theta|\cdot(1-\exp(-t/\tau_m))}{d\cdot\tau_{pol}} \tag{A12}$$

where E is the stationary value of the external field strength. At small values of $E \leq 5\ \mathrm{MV\ m^{-1}}$, where $f_\lambda \approx 1$ (practically no ME yet), the integration of Eq. (A12) yields:

$$\begin{aligned} E_m(t) = {} & \frac{1.5\cdot E\cdot a\cdot|\cos\theta|\cdot\exp\left(-t/\tau_{pol}\right)}{d\cdot\tau_{pol}}\int_0^t \exp\left(\vartheta/\tau_{pol}\right) \\ & \cdot(1-\exp(-\vartheta/\tau_m))\mathrm{d}\vartheta = 1.5\cdot E\cdot a\cdot|\cos\theta| \\ & \cdot\left(1-\left(\tau_{pol}\cdot\exp\left(-t/\tau_{pol}\right) - \tau_m\cdot\exp(-t/\tau_m)\right)\right. \\ & \left./\left(\tau_{pol}-\tau_m\right)\right)/d \end{aligned} \tag{A13}$$

where ϑ is the dummy time variable. The time constants τ_m and τ_{pol} permit to calculate the delay time $t_d = \tau_m + \tau_{pol}$ in the build-up of T_g and T_ℓ and, consequently, the description of the sigmoidal increase in the time course of ΔS_{MS}, ΔS_{SU} and ΔS_{ME}, respectively. Since $\tau_{MS} \ll \tau_{pol}$ and $\tau_{MS} \ll \tau_m$, see Eq. (9) of the text, substitution of $T_\ell = C_m\cdot d^2\cdot\langle E_m^2\rangle/2$, where $\langle E_m^2\rangle = \langle\Delta\varphi^2\rangle/d^2$, see Eq. (A13), into Eq. (10) yields Eq. (18) of the text. Note, even if $\tau_{pol} \gg \tau_m$, Eq. (18) represents a sigmoidal increase in ΔS_{MS}, because of the quadratic term $(1-\exp(-t/\tau_{pol}))^2$.

The build-up of the global stress T_g (Eq. (A8)) depends on the build-up of the global polarization of the vesicle (τ_m) and on the decay phase of the displacement current across the membrane (τ_{pol}). Actually, as long as the electrical membrane condenser is not completely charged, the membrane is conductive and the global polarization of the vesicle is not fully established.

Applying Eq. (A12), the displacement current density j_m^d of the current $I = \mathrm{d}q/\mathrm{d}t$ through the membrane is given by:

$$\begin{aligned} j_m^d &= \frac{\mathrm{d}q}{S_0\cdot\mathrm{d}t} = C_m\cdot d\cdot\frac{\mathrm{d}E_m}{\mathrm{d}t} \\ &= 1.5\cdot E\cdot a\cdot|\cos\theta|\cdot C_m\frac{\exp\left(-t/\tau_{pol}\right) - \exp(-t/\tau_m)}{\tau_{pol}-\tau_m} \end{aligned} \tag{A14}$$

The membrane conductivity λ_m^d due to the displacement current density, $j_m^d = \lambda_m^d \cdot E_m$, is given by:

$$\lambda_m^d = \frac{j_m^d}{E_m} = \frac{C_m \cdot d \cdot \left(\exp\left(-t/\tau_{pol}\right) - \exp\left(-t/\tau_m\right)\right)}{\tau_{pol} - \tau_m - \left(\tau_{pol} \cdot \exp\left(-t/\tau_{pol}\right) - \tau_m \cdot \exp\left(-t/\tau_m\right)\right)}. \quad \text{(A15)}$$

The total membrane conductivity is given by $\lambda_m = \sqrt{\left(\lambda_m^d\right)^2 + \left(\lambda_m^0\right)^2}$, where λ_m^0 is the real part of the membrane conductivity. For the closed (non-electroporated) lipid membrane $\lambda_m^0 = 5 \cdot 10^{-13}$ S m^{-1} [60]. During membrane charging, the inequality $\lambda_m^d \gg \lambda_m^r$ holds and therefore $\lambda_m \approx \lambda_m^d$. At small degrees of vesicle deformation $p < 1.5$, Eq. (A8) can be approximated by $T_g = 3a \cdot \varepsilon_0 \varepsilon_w E^2/80$ and the membrane area increase due to the global tension is given by the Eq. (19) of the main text.

In most practical cases, the smoothing of thermal undulations is described by the inequality $T_g/(\pi \cdot \kappa/4a^2 + \sigma_0) \ll 1$ [61]. Thus Eq. (12) of the text simplifies to:

$$\frac{\Delta S_{SU}}{S_0} = \frac{k_B T}{8\pi\kappa} \cdot \frac{T_g}{\pi\kappa/4a^2 + \sigma_0} \quad \text{(A16)}$$

In the case when $\tau_{SU} \approx \tau_{pol}$, the kinetics of $\Delta S_{SU}(t)/S_0$ is given by the Eq. (20) of the main text.

Appendix D. Membrane electroporation parameters

The built-up of the fraction of membrane pores f_2 is explicitly calculated by insertion of Eq. (A13) for the membrane field into the kinetic rate equation:

$$\frac{df_2}{dt} + \frac{f_2}{\tau_{ME}} = \frac{f_2^0 \exp\left(b \cdot \left\langle E_m^2(t)\right\rangle\right)}{\tau_{ME}} \quad \text{(A17)}$$

Using the initial condition $f_2(t=0) = f_2^0$, we obtain the Eq. (21) of the main text.

The field dependence of the overall equilibrium constant K_2 of the poration–resealing process of ME according to Eq. (13) is given by [50]:

$$K_2 = K_2^0 \cdot \exp\left(b \cdot \left\langle E_m^2\right\rangle\right), \quad \text{(A18)}$$

where $K_2^0 = K_2(E_m = 0)$ and

$$b = \pi \cdot \varepsilon_0 \cdot (\varepsilon_w - \varepsilon_L) \cdot \bar{r}_p^2 \cdot d/(2k_B T), \quad \text{(A19)}$$

where $\bar{r}_p$ is the mean pore radius. It is recalled that in the initial time range of $t \le \tau_{pol}$, the induced average membrane field term $\langle E_m^2 \rangle$ depends on time due to the ionic polarization; Eq. (A13).

References

[1] R.A. Demel, B. De Kruyff, The function of sterols in membranes, Biochim. Biophys. Acta 457 (1976) 109–132.
[2] P.L. Yeagle, Cholesterol and the cell membrane, Biochim. Biophys. Acta 822 (1985) 267–287.
[3] J.B. Finean, Interaction between cholesterol and phospholipid in hydrated bilayers, Chem. Phys. Lipids 54 (1990) 147–156.
[4] T. Gilat, G.J. Sömjen, Phospholipid vesicles and other cholesterol carriers, Biochim. Biophys. Acta 1286 (1996) 95–115.
[5] G.H. Addona, J.H. Sandermann, M.A. Kloczewiak, S.S. Husain, K.W. Miller, Where does cholesterol act during activation of the nicotinic acetylcholine receptor? Biochim. Biophys. Acta 1370 (1998) 299–309.
[6] K. Simons, E. Ikonen, Functional rafts in cell membranes, Nature 387 (1997) 569–572.
[7] R. Varma, S. Mayor, GPI-anchored proteins are organized in submicron domains at the cell surface, Nature 394 (1998) 798–801.
[8] T. Friedrichson, T. Kurzchalia, Microdomains of GPI-anchored proteins in living cells revealed by crosslinking, Nature 394 (1998) 802–805.
[9] D. Needham, T.J. McIntosh, E. Evans, Thermomechanical and transition properties of dimiristoylphosphatidylcholine/cholesterol bilayers, Biochemistry 27 (1988) 4668–4673.
[10] D. Needham, R.S. Nunn, Elastic deformation and failure of lipid bilayer membranes containing cholesterol, Biophys. J. 58 (1990) 997–1009.
[11] J. Song, R.E. Waugh, Bending rigidity of SOPC membranes containing cholesterol, Biophys. J. 71 (1993) 1967–1970.
[12] U. Seifert, R. Lipowsky, in: R. Lipowsky, E. Sackmann (Eds.), Handbook of Biological Physics: Structure and Dynamics of Membrane, Morphology of Vesicles, vol. 1A, Elsevier Science B.V, Amsterdam, 1995, p. 403.
[13] E. Sackmann, in: R. Lipowsky, E. Sackmann (Eds.), Handbook of Biological Physics: Structure and Dynamics of Membrane, Physical Basis of Self-Organization and Function of Membranes: Physics of Vesicles, vol. 1A, Elsevier Science B.V, Amsterdam, 1995, p. 213.
[14] A.M. Smondyrev, M.L. Berkowitz, Structure of dipalmitoylphosphatidylcholine/cholesterol bilayer at low and high cholesterol concentrations: molecular dynamics simulations, Biophys. J. 77 (1999) 2075–2089.
[15] F.A. Nezil, M. Bloom, Combined influence of cholesterol and synthetic amphiphillic peptides upon bilayer thickness in model membranes, Biophys. J. 61 (1992) 1176–1183.
[16] Ch. Paré, M. Lafler, Polymorphism of POPE/cholesterol system: a 2H nuclear magnetic resonance and infrared spectroscopic investigation, Biophys. J. 74 (1998) 899–909.
[17] L. Beney, J.M. Perrier-Cornet, M. Hayert, P. Gervais, Shape modification of phospholipid vesicles induced by high pressure: influence of bilayer compressibility, Biophys. J. 72 (1997) 1258–1263.
[18] C. Bernsdorff, A. Wolf, R. Winter, E. Gratton, Effect of hydrostatic pressure on water penetration and rotational dynamics in phospholipid–cholesterol bilayers, Biophys. J. 72 (1997) 1264–1277.
[19] M. Straume, B.J. Litman, Influence of cholesterol on equilibrium and dynamic bilayer structure of unsaturated acyl chain phosphtidylcholine vesicles as determined from higher order analysis of fluorescence anisotropy decay, Biochemistry 26 (1987) 5121–5126.
[20] M. Antunes-Madeira, R.A. Videira, M.L. Klüppel, V.V. Madeira, Amidorane effects on membrane organization evaluated by fluorescence polarization, Int. J. Cardiol. 48 (1995) 211–218.
[21] T.P.W. McMullen, R.N. McElhaney, New aspects of the interaction of cholesterol with dipalmitoylphosphatidylcholine bilayers as revealed by high-sensitivity differential scanning calorimetry, Biochim. Biophys. Acta 1234 (1995) 90–98.
[22] M.B. Sankaram, T.E. Thompson, Modulation of phospolipid acyl chain order by cholesterol. A solid-state ^{2}H nuclear magnetic resonance study, Biochemistry 29 (1990) 10676–10684.

[23] E. Neumann, M. Schaefer-Ridder, Y. Wang, P.H. Hofschneider, Gene transfer into mouse lyoma cells by electroporation in high electric fields, EMBO J. 1 (1982) 841–845.
[24] E. Neumann, K. Rosenheck, Permeability changes induced by electric impulses in vesicular membranes, J. Membr. Biol. 10 (1972) 279–290.
[25] E. Neumann, S. Kakorin, Digression on membrane electroporation and electroporative delivery of drugs and genes, Radiol. Oncol. 32 (1998) 7–17.
[26] E. Neumann, S. Kakorin, Electrooptics of membrane electroporation and vesicle shape deformation, Curr. Opin. Colloid Interface Sci. 1 (1996) 790–799.
[27] E. Neumann, S. Kakorin, K. Toensing, Membrane electroporation and electromechanical deformation of vesicle and cells, Faraday Discuss. 111 (1998) 111–125.
[28] U. Brinkmann, Effect of cholesterol and dodecylsulfate on the electroporative deformation and solubilization of lipid bilayer vesicles. PhD thesis, University of Bielefeld, 1998.
[29] K. Tönsing, S. Kakorin, E. Neumann, S. Liemann, R. Huber, Annexin V and vesicle membrane electroporation, Eur. Biophys. J. 26 (1997) 307–318.
[30] E. Neumann, S. Kakorin, Chemical electrooptics and linear dichroism of polyelectroytes and colloids, Ber. Bunsenges. Phys. Chem. 100 (1996) 721–722.
[31] S. Kakorin, E. Neumann, Kinetics of the electroporative deformation of lipid vesicles and biological cells in an electric field, Ber. Bunsenges. Phys. Chem. 102 (1998) 670–675.
[32] A. Revzin, E. Neumann, Conformational changes in rRNA induced by electric impulses, Biophys. Chemist. 2 (1974) 144–150.
[33] B. Zeks, S. Svetina, The structure and conformation of amphiphilic membranes, in: R. Lipowsky, D. Richter, K. Kremer (Eds.), The Effect of the Electric Field on the Shapes of Phospholipid Vesicles, Springer Proceedings in Physics, vol. 66, 1992, p. 174.
[34] V.G. Farafonov, N.V. Voshinnikov, V.V. Somsikov, Light scattering by a core–mantle spheroidal particle, Appl. Opt. 35 (1996) 5412–5426.
[35] T. Griese, S. Kakorin, E. Neumann, Conductometric and electrooptic relaxation spectrometry of lipid vesicle electroporation at high fields, Phys. Chem. Chem. Phys. 4 (2002) 1217–1227.
[36] S. Kakorin, E. Redeker, E. Neumann, Electroporative deformation of salt-filled lipid vesicles, Eur. Biophys. J. 27 (1998) 43–53.
[37] S. Komura, in: M. Rosoff (Ed.), Vesicles, Shape Fluctuations of Vesicles, Marcel Dekker, Inc., New York, 1996, p. 197.
[38] S. Kakorin, Th. Liese, E. Neumann, Membrane curvature and high-field electroporation of lipid bilayer vesicles, J. Phys. Chem., B 107 (2003) 10243–10251.
[39] E. Neumann, The relaxation hysteresis of membrane electroporation, in: E. Neumann, A.E. Sowers, C. Jordan (Eds.), Electroporation and Electrofusion in Cell Biology, vol. 2, Plenum Press, New York, 1989, p. 61.
[40] E. Neumann, S. Kakorin, Electroporation of curved lipid membranes in ionic strength gradients, Biophys. Chemist. 85 (2000) 249–271.
[41] M. Schmeer, Th. Seipp, U. Pliquett, S. Kakorin, E. Neumann, Mechanism for the conductivity changes caused by membrane electroporation of CHO cell—pellets, Phys. Chem. Chem. Phys. (2004) .
[42] E. Neumann, Chemical electric field effects in biological macromolecules, Prog. Biophys. Mol. Biol. 47 (1986) 197–231.
[43] L.W. Engel, F.G. Prendergast, Values for significance of order parameters and "Cone Angles" of fluorophore rotation in lipid bilayers, Biochemistry 20 (1981) 7338–7345.
[44] K. Kinosita, S. Kawato, A. Ikegami, A theory of fluorescence polarization decay in membranes, Biophys. J. 20 (1977) 289–305.
[45] C.S. Chong, K. Colbow, Light scattering and turbidity measurements on lipid vesicles, Biochim. Biophys. Acta 436 (1976) 260–282.
[46] S. Kakorin, E. Neumann, Electrooptical studies of membrane electroporation in lipid vesicles, Colloids Surf., A Physicochem. Eng. Asp. 209 (2002) 147–165.
[47] M.C. Wiener, R.M. Suter, J.F. Nagle, Structure of the fully hydrated gel phase of dipalmitoylphosphatidylcholine, Biophys. J. 55 (1989) 315–316.
[48] Th.J. McIntosh, A.D. Magid, in: G. Cevc (Ed.), Phospholipids Handbook in Library of Congress Cataloging-in-Publication Data, Phospholipid Hydration, Marcel Dekker, Inc., New York, 1993, p. 553.
[49] A. Lopez, M.P. Rols, J. Teissie, ^{31}P NMR analysis of membrane phospholipid organization in viable, reversibly electropermeabilized Chinese hamster ovary cells, Biochemistry 27 (1988) 1222–1228.
[50] S. Kakorin, S.P. Stoylov, E. Neumann, Electro-optics of membrane electroporation in diphenylhexatriene-doped lipid bilayer vesicles, Biophys. Chemist. 58 (1996) 1–7.
[51] R.M. Peitzsch, M. Eisenberg, K.A. Sharp, S. McLaughlin, Calculations of the electrostatic potential adjacent to model phospholipid bilayers, Biophys. J. 68 (1995) 729–738.
[52] Th.J. McIntosh, The effect of cholesterol on the structure of phosphatidylcholine bilayers, Biochim. Biophys. Acta 513 (1978) 43–58.
[53] T. Parasassi, M.D. Stefano, M. Loiero, G. Ravagnan, E. Gratton, Influence of cholesterol on phospholipid bilayer phase domains as detected by laurdan fluorescence, Biophys. J. 66 (1994) 120–132.
[54] T. Parasassi, M.D. Stefano, M. Loiero, G. Ravagnan, E. Gratton, Cholesterol modifies water concentration and dynamics in phospholipid bilayers: a fluorescence study using laurdan probe, Biophys. J. 66 (1994) 763–768.
[55] D. Bach, E.J. Wachtel, X-ray diffraction study of cholesterol–phosphatidylserine mixtures, Biochim. Biophys. Acta 922 (1987) 234–238.
[56] D. Bach, E.J. Wachtel, Hydration of phospholipid bilayers in the presence and absence of cholesterol, Biochim. Biophys. Acta 1368 (1998) 216–224.
[57] B. Klösgen, W. Helfrich, Special features of phosphatidylcholine vesicles as seen in cryo-transmission electron-microscopy, Eur. Biophys. J. 22 (1993) 329–340.
[58] H.P. Schwan, Electrical properties of tissue and cell suspensions, Adv. Biol. Med. Phys. 5 (1957) 147–209.
[59] M. Eigen, L. DeMayer, Relaxation methods, in: S.L. Friess, E.S. Lewis, A. Weissberger (Eds.), Techniques of Organic Chemistry, vol. 8 (2), John Wiley, New York, 1963, pp. 895–1054.
[60] G. Cevc, J. Seddon, in: G. Cevc (Ed.), Phospholipid Handbook, Marcel Dekker, Inc., New York, 1993, p. 351.
[61] W. Helfrich, R.-M. Servuss, Undulations, steric interaction and cohesion of fluid membranes, Nuovo Cim. 3D (1984) 137–151.

Glossary

K: membrane stretching modulus (N m^{-1})
f_p: surface fraction of membrane pores
f_W: volume fraction of water in the membrane
f_λ: membrane conductivity factor
n_w: refractive index of the extravesicular medium
n_m: refractive index of the lipid membrane
N_p^{ves}: average pore number in one vesicle
T_g: global Maxwell tension of membrane
T_e: A local Maxwell tension of membrane
ΔT^-, ΔT^+: turbidity "minus" and "plus" modes, respectively
ΔA^-, ΔA^+: absorbance "minus" and "plus" modes, respectively
$\bar{r}_p$: mean pore radius
ΔS: increment of the membrane surface area S
ΔS_{MS}: increment of the membrane area due to stretching
ΔS_{SU}: increment of the membrane area due to smoothing of thermal undulations
ΔS_{ME}: increment of the membrane area due to electropores
S_0: membrane initial projected surface area (at $E=0$)

t_E: duration of the rectangular electric pulse
V_0: initial vesicle volume (at $E=0$)
a: radius of projected surface of the vesicle
$p=c/b$: axis ratio of the spheroidal vesicle
E: electric field strength
E_m: electric field strength of the membrane
x: mole fraction of cholesterol in the membrane
α: orientational angle of the chromophore in the membrane
σ: membrane lateral tension
σ_0: initial membrane lateral tension (at $E=0$)
κ: membrane bending rigidity
λ_m: conductivity of the membrane
λ_{in}: conductivity of the intravesicular solution
λ_{ex}: conductivity of the extravesicular solution
τ_{MS}: characteristic time of membrane stretching
τ_{SU}: characteristic time of smoothing of thermal undulations
τ_{ME}: relaxation time of membrane electroporation
τ_{pol}: characteristic time of ionic membrane polarization
τ_m: characteristic machine time of the field-jump apparatus